Production of light (anti)nuclei in pp collisions at √s = 13 TeV

(ALICE Collaboration) Acharya, S.; ...; Erhardt, Filip; ...; Gotovac, Sven; ...; Jerčić, Marko; ...; Karatović, David; ...; ...

Source / Izvornik: **Journal of High Energy Physics, 2022, 2022**

Journal article, Published version
Rad u časopisu, Objavljena verzija rada (izdavačev PDF)

https://doi.org/10.1007/JHEP01(2022)106

Permanent link / Trajna poveznica: https://urn.nsk.hr/urn:nbn:hr:217:895343

Published for SISSA by Springer

Received: October 13, 2021
Accepted: December 13, 2021
Published: January 20, 2022

Production of light (anti)nuclei in pp collisions at $\sqrt{s} = 13$ TeV

The ALICE collaboration

E-mail: ALICE-publications@cern.ch

Abstract: Understanding the production mechanism of light (anti)nuclei is one of the key challenges of nuclear physics and has important consequences for astrophysics, since it provides an input for indirect dark-matter searches in space. In this paper, the latest results about the production of light (anti)nuclei in pp collisions at $\sqrt{s} = 13$ TeV are presented, focusing on the comparison with the predictions of coalescence and thermal models. For the first time, the coalescence parameters B_2 for deuterons and B_3 for helions are compared with parameter-free theoretical predictions that are directly constrained by the femtoscopic measurement of the source radius in the same event class. A fair description of the data with a Gaussian wave function is observed for both deuteron and helion, supporting the coalescence mechanism for the production of light (anti)nuclei in pp collisions. This method paves the way for future investigations of the internal structure of more complex nuclear clusters, including the hypertriton.

Keywords: Hadron-Hadron scattering (experiments)

ArXiv ePrint: 2109.13026

https://doi.org/10.1007/JHEP01(2022)106

Contents

JHEP01(2022)106

1 Introduction

In high-energy hadronic collisions at the LHC, the production of light (anti)nuclei and more complex multi-baryon bound states, such as (anti)hypertriton [1], is observed. An unexpectedly large yield of light nuclei was observed for the first time in proton-nucleus collisions at the CERN PS accelerator [2]. Twenty-five years later, the study of nuclear production was carried out at Brookhaven AGS and at CERN SPS, with the beginning of the program of relativistic nuclear collisions [3]. Extensive studies of the production of light (anti)nuclei were later performed at the Relativistic Heavy-Ion Collider (RHIC) [4–7], including the first observation of an antihypernucleus [8] and of anti(alpha) [9]. In this paper, the focus will be on results obtained at LHC. The production yields of light

(anti)nuclei have been measured as a function of transverse momentum (p_{T}) and charged-particle multiplicity in different collision systems and at different center-of-mass energies by ALICE [10–17]. One of the most interesting observations obtained from such a large variety of experimental data is that the production of light (anti)nuclei seems to depend solely on the charged-particle multiplicity (hereinafter denoted multiplicity). This observation manifests itself in the continuous evolution of the deuteron-to-proton (d/p) and ^{3}He-to-proton (^{3}He/p) ratios with the event multiplicity across different collision systems and energies [16, 17]. The results presented in this paper complement the existing picture, providing measurements in yet unexplored multiplicity regions.

These measurements have an important astrophysical value as they provide input for the background estimates in indirect dark matter searches in space. Indeed, only small systems like pp collisions are relevant for such searches because the interstellar medium consists mostly of hydrogen (protons) and helium (alpha particles). In this context, the observation of a significant antimatter excess with respect to the expected background of antimatter produced in ordinary cosmic ray pp or p-alpha interactions would represent a signal for dark matter annihilation in the galactic halo or for the existence of antimatter islands in our universe [18–21].

The theoretical description of the production mechanism of (anti)nuclei is still an open problem and under intense debate in the scientific community. Two phenomenological models are typically used to describe the production of multi-baryon bound states: the statistical hadronisation model (SHM) [22–28] and the coalescence model [29–34]. In the former, light nuclei are assumed to be emitted by a source in local thermal and hadrochemical equilibrium and their abundances are fixed at chemical freeze-out. The version of this model using the grand-canonical ensemble reproduces the light-flavoured hadron yields measured in central nucleus-nucleus collisions, including those of (anti)nuclei and (anti)hypernuclei [22]. In pp and p-Pb collisions, the production of light nuclei can be described using a different implementation of this model based on the canonical ensemble, where exact conservation of the electric charge, strangeness, and baryon quantum numbers is applied within a pre-defined correlation volume [25, 28]. In the coalescence model, light nuclei are assumed to be formed by the coalescence of protons and neutrons which are close in phase space at kinetic freeze-out [30]. In the most simple version of this model, nucleons are treated as point-like particles and only correlations in momentum space are considered, i.e. the bound state is assumed to be formed if the difference between the momenta of nucleons is smaller than a given threshold p_0, a free parameter of the model which is typically of the order of 100 MeV/c. This simple version of the coalescence model can approximately reproduce deuteron production data in low-multiplicity collisions and was recently used to describe the jet-associated deuteron p_{T}-differential yields in pp collisions at $\sqrt{s}$ =13 TeV [35]. In recent developments [31, 36], the quantum-mechanical properties of nucleons and nuclei are taken into account and the coalescence probability is calculated from the overlap between the source function of the emitted protons and neutrons, which are mapped on the Wigner density of the nucleus. This state-of-the-art coalescence model describes the d/p and ^{3}He/p ratios measured in different collision systems as a function of multiplicity [33]. On the contrary, the simple coalescence approach provides a description

JHEP01(2022)106

of p_{T} spectra of light (anti)nuclei measured in high-energy hadronic collisions only in the low-multiplicity regime [15].

In this paper, the measurement of the production yields of light (anti)nuclei in pp collisions at $\sqrt{s}$ =13 TeV are presented. In particular, part of the results is obtained from data collected with a high-multiplicity trigger (see section 2), accessing a multiplicity typically obtained in p-Pb and peripheral Pb-Pb collisions. For the first time, the yields of (anti)nuclei are measured in a multiplicity region in which high-precision femtostopic measurements of the source size [37] are available. This allows for a parameter-free comparison of the coalescence measurements with theoretical calculations, showing the potential of this technique to set constraints on the wave function of (anti)nuclei.

2 Detector and data sample

A detailed description of the ALICE apparatus and its performance can be found in refs. [38] and [39]. The trajectories of charged particles are reconstructed in the ALICE central barrel with the Inner Tracking System (ITS) [40] and the Time Projection Chamber (TPC) [41]. The ITS consists of six cylindrical layers of silicon detectors and the two innermost layers form the Silicon Pixel Detector (SPD). The ITS is used for the reconstruction of primary and secondary vertices and of charged-particle trajectories. The TPC is used for track reconstruction, charged-particle momentum measurement and for charged-particle identification via the measurement of their specific energy loss ($\mathrm{d}E/\mathrm{d}x$) in the TPC gas [39]. Particle identification at high momentum is complemented by the time-of-flight measurement provided by the TOF detector [42]. The aforementioned detectors are located inside a large solenoid magnet, which provides a homogeneous magnetic field of 0.5 T parallel to the beam line, and cover the pseudorapidity interval $|\eta|< 0.9$. Collision events are triggered by two plastic scintillator arrays, V0C and V0A [43], located along the beam axis of the interaction point, covering the pseudorapidity regions $-3.7 < \eta < -1.7$ and $2.8 < \eta < 5.1$, respectively. The signals from V0A and V0C are summed to form the V0M signal, which is used to define event classes to which the measured multiplicity is associated [44]. Moreover, the timing information of the V0 detectors is used for the offline rejection of events triggered by interactions of the beam with the residual gas in the LHC vacuum pipe.

The results presented in this paper are obtained from data collected in 2016, 2017 and 2018, both with minimum bias (MB) and high multiplicity (HM) triggers. For the minimum-bias event trigger, coincident signals in both V0 scintillators are required to be synchronous with the beam crossing time defined by the LHC clock. Events with high charged-particle multiplicities are triggered on by additionally requiring the total signal amplitude measured in the V0 detector to exceed a threshold. At the analysis level, the 0–0.1% percentile of inelastic events with the highest V0 multiplicity (V0M) is selected to define the high-multiplicity event class. Events with multiple vertices identified with the SPD are tagged as pile-up in the same bunch crossing (in-bunch pile-up) and removed from the analysis [39]. Assuming that all the in-buch pile-up is in the 0–0.01% percentile of inelastic events, which is the worst-case scenario, only 3% of the selected events (in the 0–0.01% percentile) would be pile-up events. Therefore, the effect of in-bunch pile-up

JHEP01(2022)106

on the production spectra is negligible. Pile-up in different bunch crossings, instead, is rejected by requiring track hits in the SPD and its contribution is negligible. The data sample consists of approximately 2.6 billion MB events and 650 million HM events.

For the measurements of (anti)protons and (anti)deuterons, the high-multiplicity data sample is divided into three multiplicity classes: HM I, HM II and HM III. The multiplicity classes are determined from the sum of the signal amplitudes measured by the V0 detectors and defined in terms of the percentiles of the INEL > 0 pp cross section, where an INEL > 0 event is a collision with at least a charged particle in the pseudorapidity region $|\eta| < 1$ [45]. For this purpose, charged particles are measured with SPD tracklets, obtained from a pair of hits in the first and second layer of the SPD, respectively. In the case of (anti)triton (^{3}H) and (anti)helion (^{3}He), due to their lower production rate, it is not possible to divide the HM sample into smaller classes, but for (anti)helion the MB sample is divided into two multiplicity classes, MB I and MB II, defined from the percentiles of the INEL > 0 pp cross section. The average charged particle multiplicity $\langle \mathrm{d}N_{\mathrm{ch}}/\mathrm{d}\eta \rangle$ for all the multiplicity classes will be reported in table 2. It is defined as the number of primary charged particles produced in the pseudorapidity interval $|\eta| < 0.5$. A detailed description of the $\langle \mathrm{d}N_{\mathrm{ch}}/\mathrm{d}\eta \rangle$ estimation can be found in ref. [46].

3 Data analysis

3.1 Track selection

(Anti)nuclei candidates are selected from the charged-particle tracks reconstructed in the ITS and TPC in the pseudorapidity interval $|\eta| < 0.8$. The criteria used for track selection are the same as reported in ref. [17]. Particle identification is performed using the $\mathrm{d}E/\mathrm{d}x$ measured by the TPC and the time-of-flight measured by the TOF. For the TPC analysis, the signal is obtained from the $n\sigma_{\mathrm{TPC}}$ distribution, where $n\sigma_{\mathrm{TPC}}$ is the difference between the measured and expected signals for a given particle hypothesis, divided by the resolution. For the TOF analysis, the yield in each p_{T} interval is extracted from the distribution of the TOF squared-mass, defined as $m^2 = p^2\,(t^2_{\mathrm{TOF}}/L^2 - 1/c^2)$, where t_{TOF} is the measured time-of-flight, L is the length of the track and p is the momentum of the particle. Similarly to the TPC case, one defines $n\sigma_{\mathrm{TOF}}$ as the difference between the measured and expected time of flight for a given particle hypothesis, divided by the resolution. For the TOF analysis, a pre-selection based on the measured TPC $\mathrm{d}E/\mathrm{d}x$ ($|n\sigma_{\mathrm{TPC}}| < 3$) is performed to reduce the background originating from other particle species. More details about particle identification with TPC and with TOF can be found in ref. [17].

The (anti)deuteron yield is extracted from the TPC signal for $p_{\mathrm{T}} < 1\,\mathrm{GeV}/c$, while at higher p_{T} the yield is extracted from the TOF after the pre-selection using the TPC signal. For (anti)protons, the TOF is used for the entire p_{T} range. (Anti)tritons are identified through the TPC signal and after a pre-selection with TOF ($|n\sigma_{\mathrm{TOF}}| < 3$) for $p_{\mathrm{T}} < 2\,\mathrm{GeV}/c$. The (anti)helion identification is based only on the TPC $\mathrm{d}E/\mathrm{d}x$, which provides a good separation of its signal from that of other particle species. This is due to the charge Z $= 2$ of this nucleus.

JHEP01(2022)106

3.2 Efficiency and acceptance correction

The estimation of reconstruction efficiencies of both nuclei and antinuclei, as well as those of the contamination to the raw p_{T} spectra of nuclei from spallation and of the signal loss due to event selection, requires Monte Carlo (MC) simulations. Simulated pp collision events, generated using Pythia 8 [47] (Monash 2013 tune [48]), are enriched by an injected sample of (anti-)nuclei generated with a flat p_{T} distribution in the transverse-momentum range $0 < p_{\mathrm{T}} < 10$ GeV/c and a flat rapidity distribution in the range $|y| < 1$. The interactions of the generated particles with the experimental apparatus are modeled by GEANT4 [49]. The detector conditions during the data taking are reproduced in the simulations.

The raw p_{T} spectra of (anti)nuclei are corrected for the reconstruction efficiency and acceptance, defined as

$$\epsilon(p_{\mathrm{T}}) = \frac{N_{\mathrm{rec}}(|\eta| < 0.8, |y| < 0.5, p_{\mathrm{T}}^{\mathrm{rec}})}{N_{\mathrm{gen}}(|y| < 0.5, p_{\mathrm{T}})}, \tag{3.1}$$

where N_{rec} and N_{gen} are the number of reconstructed and generated (anti)nuclei, respectively. The same criteria for the track selection and particle identification used in the real data analysis are applied to reconstructed tracks in the simulation. Considering that (anti)nuclei are injected with a flat p_{T} distribution into the simulated events, their input distributions are reshaped using p_{T}-dependent weights to match the real shape observed in data. The latter is parameterised using a Lévy-Tsallis function whose parameters are determined using an iterative procedure: they are initialized using the values taken from ref. [17], the corrected spectrum is then fitted with the same function and a new set of parameters is determined and used for the next iteration. The parameters are found to converge after two iterations, with differences from the previous one of less than one per mille. Protons are abundantly produced by Pythia 8 and their spectral shape is consistent with the one obtained in real data. For this reason, (anti)protons are not injected additionally into the simulation and their shape is not modified.

3.3 Fraction of primary nuclei

Secondary nuclei are produced in the interaction of particles with the detector material. To obtain the yields of primary nuclei produced in a collision, the number of secondaries must be subtracted from the measured yield. Since the production of secondary antinuclei is extremely rare, this correction is applied only to nuclei and not to antinuclei. For (anti)protons, instead, also a contribution from weak decays of heavier unstable particles (for example Λ hyperons) is present and cannot be neglected. The fraction of primary nuclei is evaluated using different techniques according to the analysis.

For deuterons and (anti)protons, the primary fraction is obtained by fitting the distribution of the measured distance of closest approach to the primary vertex in the transverse plane (DCA_{xy}). For the fit, templates obtained from MC are used, as described in ref. [10]. The DCA_{xy} distribution of anti-deuterons is used as a template for primary deuterons considering the negligible feed-down from weak decays of hypertriton. The production of secondary deuterons is more relevant at low p_{T} (at $p_{\mathrm{T}} = 0.7\,\mathrm{GeV}/c$ the fraction of secondary deuterons is $\sim 40\%$), decreases exponentially with the transverse momentum (<

JHEP01(2022)106

5% for $p_{\rm T} = 1.4\,{\rm GeV}/c$) and becomes negligible for $p_{\rm T} > 1.6\,{\rm GeV}/c$. For the (anti)proton analysis, all the templates are taken from MC. In this case, also a template for weak decay is used. The fraction of secondary protons from material is maximum at low transverse momentum (∼5% for $p_{\rm T} = 0.4\,{\rm GeV}/c$) and decreases exponentially, becoming negligible for $p_{\rm T} > 1\,{\rm GeV}/c$. Also, the fraction of secondary (anti)protons from weak decays is maximum at low transverse momentum (∼30% for $p_{\rm T} = 0.4\,{\rm GeV}/c$) and decreases exponentially (∼10% for $p_{\rm T} = 5\,{\rm GeV}/c$).

For helion and triton, the primary fraction is obtained by fitting the ${\rm DCA}_{xy}$ distribution with two Gaussian functions with different widths, one for the primary and one for the secondary nuclei, respectively. The spallation background is also fitted using a parabola and a constant function to estimate the systematic uncertainties. For the latter, variations of the binning and fit range are also considered. A smooth function can be used in this case, considering that the peak in the ${\rm DCA}_{xy}$ distribution of secondary nuclei, which typically appears close to zero and is caused by the wrong association of one SPD cluster to the track during reconstruction, is negligible for $p_{\rm T} > 1.5\,{\rm GeV}/c$. The fraction of secondary helions and tritons, for both MB and HM pp collisions, are found to be about 15% in the $p_{\rm T}$ interval $1.5 < p_{\rm T} < 2\,{\rm GeV}/c$, about 3% in the $p_{\rm T}$ interval $2 < p_{\rm T} < 2.5\,{\rm GeV}/c$ and negligible for higher $p_{\rm T}$. For tritons and helions, only antinuclei are used for $p_{\rm T} < 1.5\,{\rm GeV}/c$, where the secondary fraction for nuclei becomes large and it is difficult to constrain the value of the correction.

3.4 Systematic uncertainties

A summary of the systematic uncertainties for all the measurements is reported in table 1. Values are provided for low ($1.5\,{\rm GeV}/c$) and high ($4\,{\rm GeV}/c$) transverse momentum. Where the systematic uncertainty differs between matter and antimatter, the latter is reported within brackets. The first source of systematic uncertainty is related to track selection. This source takes into account the imprecision in the description of the detector response in the MC simulation. The uncertainties are evaluated by varying the relevant selection criteria, as done in ref. [11]. It is worth mentioning that at low $p_{\rm T}$ uncertainties are generally larger for matter than for antimatter, due to the increasing number of secondary nuclei selected when loosing the selection on the DCA. It is one of the main sources. The second source is related to signal extraction. It is evaluated by changing the fit function used to evaluate the raw yield or, when the direct count is used, by varying the interval in which the count is performed (see ref. [11] and ref. [17] for further details). Its value increases with transverse momentum. The effect of the incomplete knowledge of the material budget of the detector is evaluated by comparing different MC simulations in which the material budget is varied by ±4.5%. This value corresponds to the uncertainty on the determination of the material budget by measuring photon conversions [39]. Similarly, the limited precision in the measurements of inelastic cross sections of (anti)nuclei with matter is a source of systematic uncertainty. It is evaluated by comparing experimental measurements of the inelastic cross section with the values implemented in GEANT4, following the same approach used in ref. [50]. For antihelion, the difference between the momentum-dependent inelastic cross sections implemented in GEANT3 [51] and GEANT4 is also considered. This

JHEP01(2022)106

Source	$p_{\mathrm{T}} = 1.5\,\mathrm{GeV}/c$				$p_{\mathrm{T}} = 4\,\mathrm{GeV}/c$		
	p ($\overline{\mathrm{p}}$)	d ($\overline{\mathrm{d}}$)	^{3}He ($^3\overline{\mathrm{He}}$)	^{3}H ($^3\overline{\mathrm{H}}$)	p ($\overline{\mathrm{p}}$)	d ($\overline{\mathrm{d}}$)	^{3}He ($^3\overline{\mathrm{He}}$)
Track selection	3%	1%	14% (10%)	14% (10%)	3%	2%	10% (7%)
Signal extraction	<1%	3%	13% (<1%)	<1%	5%	2%	<1%
Material budget	1%	1%	2%	2%	1%	<1%	2%
Hadronic interaction	1% (2%)	2% (6%)	1% (2%)	9% (6%)	1% (2%)	2% (6%)	1% (1%)
ITS-TPC matching	2%	2%	2%	2%	2%	2%	2%
TPC-TOF matching	3%	2%	–	3%	3%	2%	–
Total	6% (7%)	4% (7%)	22% (11%)	20% (17%)	7% (8%)	4% (7%)	8%

Table 1. Summary of the main contributions to the systematic uncertainties for all the particle species under study at $p_{\mathrm{T}} = 1.5\,\mathrm{GeV}/c$ and at $p_{\mathrm{T}} = 4\,\mathrm{GeV}/c$. Values in brackets refer to antiparticles. If they are not present, the systematic uncertainty is the same for particles and antiparticles. A dash symbol is used where the uncertainty from the corresponding source is not applicable. More details about the sources of the uncertainties can be found in the text.

contribution is maximum (3%) for $p_{\mathrm{T}} < 1.5\,\mathrm{GeV}/c$ and decreases to a negligible level going to higher p_{T}. Finally, the last sources of systematic uncertainty are related to the matching of the tracks between ITS and TPC and between TPC and TOF. They are evaluated from the difference between the ITS-TPC (TPC-TOF) matching in data and MC.

4 Results and discussion

The production spectra for all the species under study are shown in figure 1. The multiplicity classes used for this measurement are reported in Tab 2, together with the corresponding p_{T}-integrated yields. (Anti)protons, (anti)deuterons and (anti)helions are fitted with a Lévy-Tsallis function [52], which is used to extrapolate the yields in the unmeasured p_{T} region. For (anti)triton, the fit parameters (except for the mass and the normalisation) are fixed to those of (anti)helion, due to the few data points available. The extrapolation amounts to about 20% of the total p_{T}-integrated yield for (anti)protons and (anti)deuterons, about 30% for (anti)helions, and about 50% for (anti)tritons. Alternative fit functions such as a simple exponential depending on m_{T}, a Boltzmann function or a Blast-wave function [53–55], are used to evaluate the systematic uncertainty on the p_{T}-integrated yield as done in refs. [15–17]. This uncertainty varies between 0.5% and 3% for protons, deuterons and helions in the HM analysis. For tritons it is around 8% due to the narrower p_{T} coverage. In the MB analysis, it is around 8% (14%) for helions (tritons).

JHEP01(2022)106

Multiplicity	$\langle \mathrm{d}N_{\mathrm{ch}}/\mathrm{d}\eta \rangle_{\lvert\eta_{\mathrm{lab}}\rvert<0.5}$	$\mathrm{d}N/\mathrm{d}y$			
		p	d	^{3}He	^{3}H
HM	31.5 ± 0.3	0.80 ± 0.01 ± 0.05		$(23.3 \pm 1 \pm 3) \times 10^{-7}$	$(25 \pm 2 \pm 4) \times 10^{-7}$
HM I	35.8 ± 0.5	0.91 ± 0.01 ± 0.05	$(22.1 \pm 0.1 \pm 1.4) \times 10^{-4}$		
HM II	32.2 ± 0.4	0.83 ± 0.01 ± 0.05	$(19.8 \pm 0.1 \pm 1.3) \times 10^{-4}$		
HM III	30.1 ± 0.4	0.77 ± 0.01 ± 0.04	$(18.4 \pm 0.1 \pm 1.1) \times 10^{-4}$		
MB	6.9 ± 0.1			$(2.4 \pm 0.3 \pm 0.4) \times 10^{-7}$	$(1.7 \pm 0.3 \pm 0.4) \times 10^{-7}$
MB I	18.7 ± 0.3			$(11 \pm 2 \pm 2) \times 10^{-7}$	
MB II	6.0 ± 0.2			$(1.5 \pm 0.2 \pm 0.3) \times 10^{-7}$	

Table 2. Multiplicity classes for the different measurements, with the corresponding multiplicity $\langle \mathrm{d}N_{\mathrm{ch}}/\mathrm{d}\eta \rangle_{\lvert\eta_{\mathrm{lab}}\rvert<0.5}$, and p_{T}-integrated yields $\mathrm{d}N/\mathrm{d}y$ for the different species (average for particle and antiparticle). For $\langle \mathrm{d}N_{\mathrm{ch}}/\mathrm{d}\eta \rangle_{\lvert\eta_{\mathrm{lab}}\rvert<0.5}$, only the systematic uncertainty is reported, because the statistical one is negligible. For $\mathrm{d}N/\mathrm{d}y$, the first uncertainty is statistical and the second is systematic.

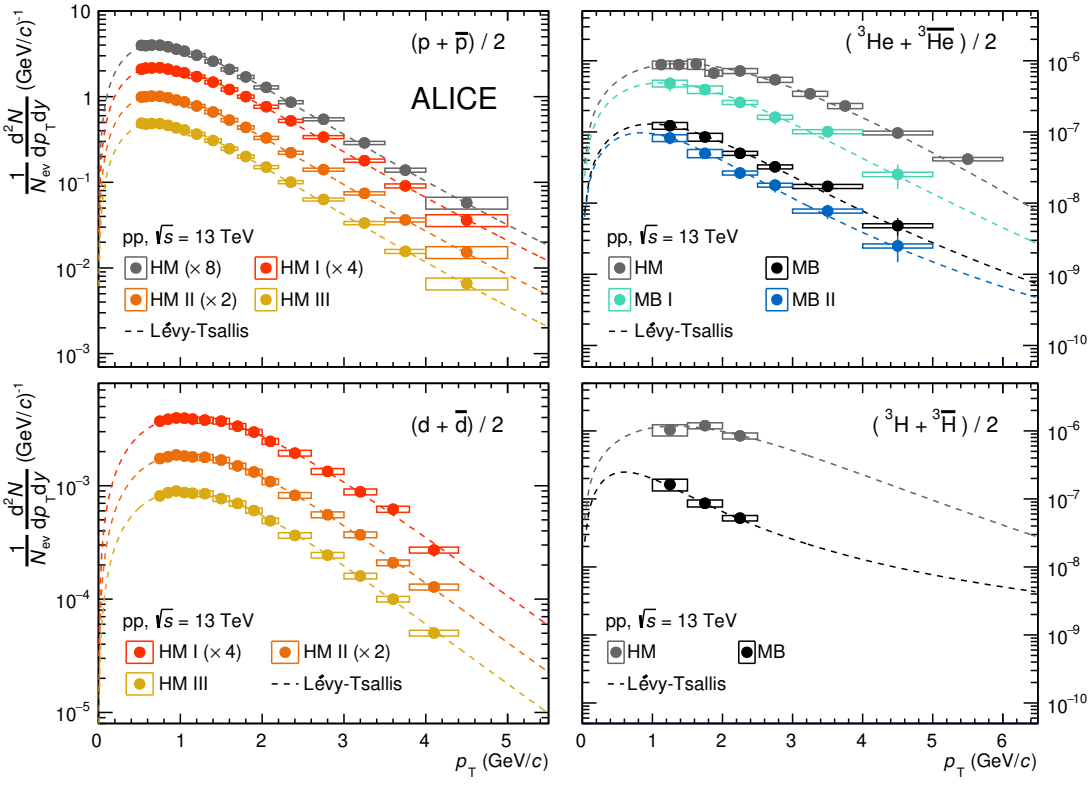

Figure 1. Transverse-momentum spectra of (anti)protons, (anti)deuterons, (anti)helion, and (anti)triton, measured in HM and MB pp collisions at $\sqrt{s} = 13$ TeV at midrapidity ($|y|< 0.5$). The results are shown in the multiplicity classes reported in table 2. Vertical bars and boxes represent statistical and systematic uncertainties, respectively. The dashed lines are individual fits with a Lévy-Tsallis function.

JHEP01(2022)106

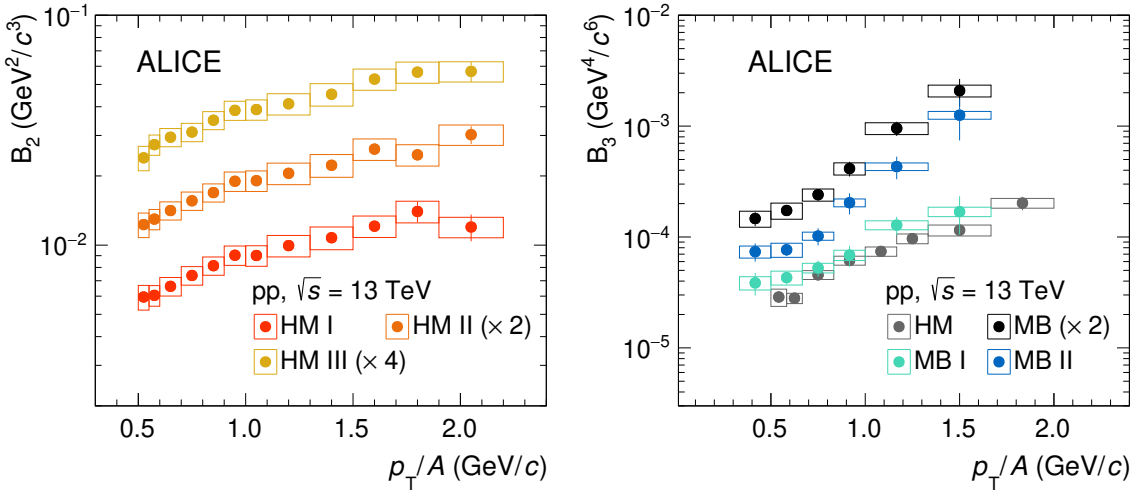

(a) (Anti)deuterons.

(b) (Anti)helions.

Figure 2. Coalescence parameters B_2 (a) and B_3 (b) as a function of p_T/A for the multiplicity classes reported in table 2. Vertical bars and boxes represent statistical and systematic uncertainties, respectively.

4.1 Coalescence parameter as a function of transverse momentum

In the coalescence model, the production probability of a nucleus with mass number A is proportional to the coalescence parameter B_A, defined as

$$B_A\left(p_{\mathrm{T}}^{\mathrm{p}}\right) = \frac{1}{2\pi p_{\mathrm{T}}^{\mathrm{A}}} \frac{\mathrm{d}^2 N_{\mathrm{A}}}{\mathrm{d}y \mathrm{d}p_{\mathrm{T}}^{\mathrm{A}}} \Bigg/ \left(\frac{1}{2\pi p_{\mathrm{T}}^{\mathrm{p}}} \frac{\mathrm{d}^2 N_{\mathrm{p}}}{\mathrm{d}y \mathrm{d}p_{\mathrm{T}}^{\mathrm{p}}}\right)^A, \tag{4.1}$$

where the labels p and A refer to protons and the (anti)nucleus with mass-number A, respectively. The invariant spectra of the (anti)protons are evaluated at the transverse momentum of the (anti)nucleus, divided by the mass-number A. For (anti)deuterons, for example, $B_A = B_2$ and $p_{\mathrm{T}}^{\mathrm{p}} = p_{\mathrm{T}}^{\mathrm{A}}/A = p_{\mathrm{T}}^{\mathrm{d}}/2$.

The coalescence parameters for (anti)deuterons (B_2) and for (anti)helions (B_3) are shown in figure 2 as a function of p_{T}/A for different multiplicity classes. Some of the measurements are scaled for better visibility (see the legend), but for B_2 the three curves are consistent with each other. A clear increase of both B_2 and B_3 with increasing p_{T}/A is observed. Previous measurements of B_2 in pp [11, 17] and p-Pb [15] collisions indicated an almost flat trend with p_{T}/A. However, in ref. [17] and in ref. [11] it was shown that even though B_2 evaluated in multiplicity classes was flat, B_2 evaluated in the multiplicity-integrated sample showed a rise with p_{T}/A. The trend shown in ref. [11] is a consequence of the mathematical definition of B_2 and of the hardening of the proton spectra. Given the narrow multiplicity intervals used in the present measurement, the significant rise of the coalescence parameters with p_{T}/A cannot be attributed to effects originating from a different hardening of the (anti)proton and (anti)nuclei spectra within these multiplicity intervals [11].

JHEP01(2022)106

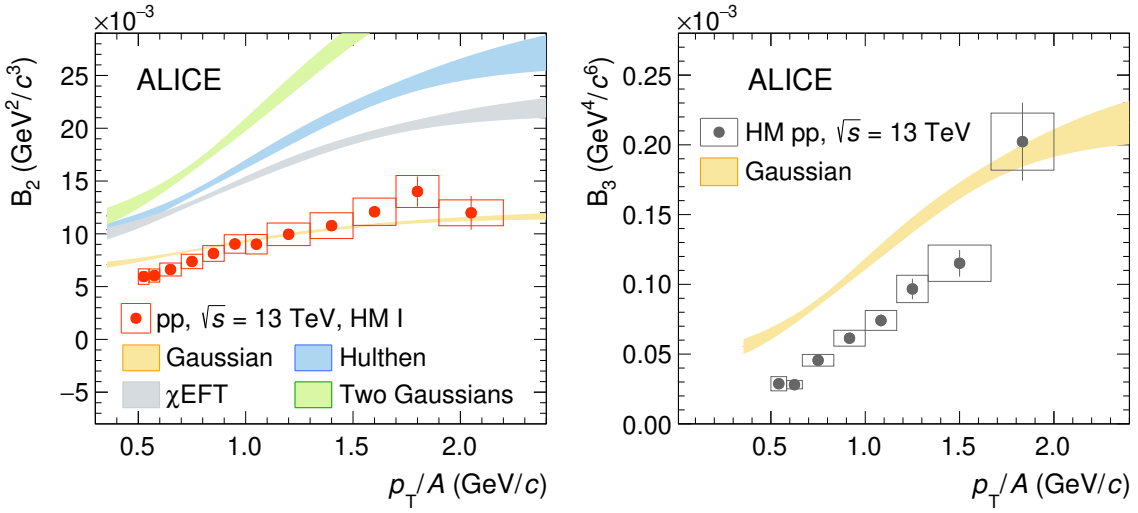

(a) (Anti)deuterons.

(b) (Anti)helions.

Figure 3. Comparison between measurements and theoretical predictions for the coalescence parameters B_2 for (anti)deuterons (a) and B_3 for (anti)helions (b) as a function of p_{T}/A. Vertical bars and boxes represent statistical and systematic uncertainties, respectively. Theoretical predictions are obtained using different wave functions to describe nuclei: Gaussian (yellow), Hulthen (blue), χEFT (gray) and two Gaussians (green).

The measurement of the coalescence parameter as a function of transverse momentum is compared with predictions from the coalescence model, using different nuclei wave functions [56] and the precise measurement of the source radii for the same data set [37]. In the case of (anti)deuterons, the following wave functions are used: single and double Gaussian [34], Hulthen [32], and a function obtained from chiral Effective Field Theory (χEFT) of order N4LO with a cutoff at 500 MeV [57]. For (anti)helion, only calculations using a Gaussian wave function are currently available, because the general recipe used for B_2 cannot be extended to B_3 but new calculations *ab initio* are needed. These wave functions and more details about the adopted theoretical models can be found in appendix A. In the coalescence model, the coalescence parameter depends on the radial extension of the particle emitting source [56]. The source radius is measured in HM pp collisions at $\sqrt{s} = 13$ TeV by ALICE using p-p and p-Λ correlations as a function of the mean transverse mass $\langle m_{\mathrm{T}} \rangle$ of the pair [37]. In ref. [37] two different measurements of the source radius are reported, $r_{\mathrm{effective}}$ and r_{core}, respectively. The difference between the two is that r_{core} takes into account the contributions coming from the strong decay of resonances by subtracting them. It is shown that r_{core} is universal, since it could describe simultaneously p-p and p-Λ correlations. In this analysis, r_{core} is used. The difference between r_{core} and $r_{\mathrm{effective}}$ is small: B_2 is on average 7% smaller using $r_{\mathrm{effective}}$, while B_3 is on average 20% smaller, due to the stronger dependence on the system size for $A > 2$ (see eq. (A.7)). For B_2, only the HM I class is considered, because the B_2 values in the three multiplicity classes are compatible.

The data in ref. [37] are parameterised as $r_{\mathrm{source}}(\langle m_{\mathrm{T}} \rangle) = c_0 + \exp(c_1 + c_2 \langle m_{\mathrm{T}} \rangle)$, with c_i free parameters, to map the transverse-mass to the source radius. The value of p_{T} cor-

JHEP01(2022)106

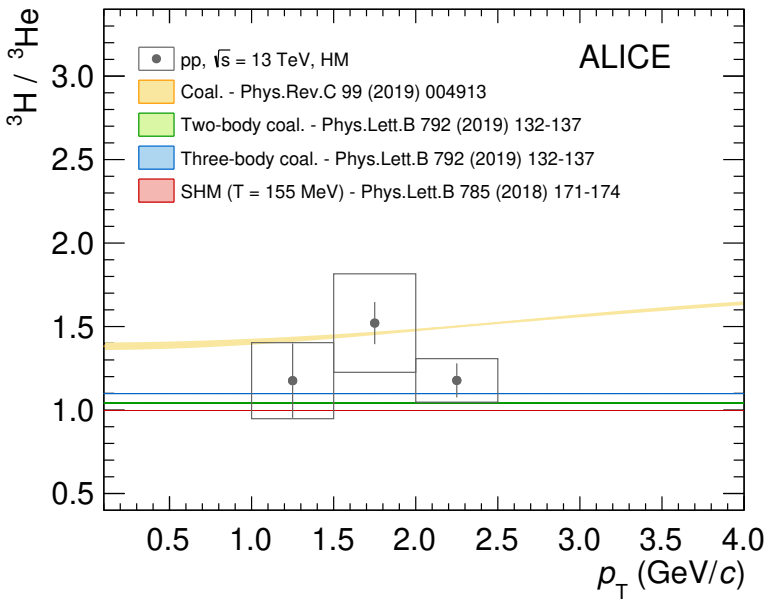

Figure 4. Ratio between the p_{T} spectra of triton and helion for the HM data sample. Vertical bars and boxes represent statistical and systematic uncertainties, respectively. The measurements are compared with the prediction of thermal (red) and coalescence models from ref. [36] (yellow) and ref. [33] (green and blue).

responding to m_{T} is taken from $m_{\mathrm{T}} = \sqrt{m_{\mathrm{p}}^2 + (p_{\mathrm{T}}/A)^2}$, where m_{p} is the proton mass. The radius of the deuteron and ^{3}He are taken from ref. [58]. The coalescence predictions are shown in comparison with the data in figure 3. Bands represent the uncertainty propagated from the measurement of the source radius. In the case of B_2, the Gaussian wave function provides the best description of the data, even though the Hulthen wave function is favoured by low-energy scattering experiments [59]. The other wave functions are significantly larger than the measurement. For the B_3, the coalescence predictions using a Gaussian wave function of helion are above the data by almost a factor of 2 except for the last p_{T} interval, which is consistent with the measured B_3 within the uncertainties. In the future, a systematic investigation of the coalescence parameter B_3 using different wave functions, in the context of the coalescence model, will gauge the potential of coalescence measurements to further constrain the wave function of helion. This technique can be used in a more general context to obtain information on the internal wave function of more complex (hyper)nuclei, such as alpha (^{4}He) and hypertriton.

4.2 Ratio between triton and helion yields

The statistical hadronisation and coalescence models predict different yields of nuclei with similar masses but different radii. To test the production model, the ratio of triton and helion is measured as a function of p_{T} for HM pp collisions (figure 4) and compared with the model predictions. Two different versions of coalescence are considered, based on ref. [33]

JHEP01(2022)106

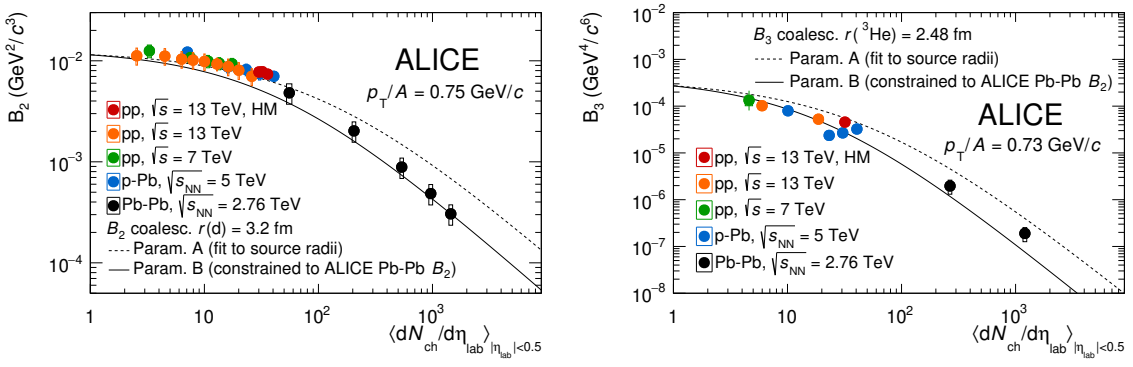

(a) (Anti)deuterons. (b) (Anti)helions.

Figure 5. (a): B_2 at $p_T/A = 0.75\,\text{GeV}/c$ as a function of multiplicity in HM pp collisions at $\sqrt{s} = 13\,\text{TeV}$, in MB pp collisions at $\sqrt{s} = 13\,\text{TeV}$ [17] and at $\sqrt{s} = 7\,\text{TeV}$ [11], in p-Pb collisions at $\sqrt{s_{\text{NN}}} = 5.02\,\text{TeV}$ [15], and in Pb-Pb collisions at $\sqrt{s_{\text{NN}}} = 2.76\,\text{TeV}$ [10]. (b): B_3 at $p_T/A = 0.73\,\text{GeV}/c$ as a function of multiplicity in HM pp collisions at $\sqrt{s} = 13\,\text{TeV}$, in MB pp collisions at $\sqrt{s} = 13\,\text{TeV}$, in p-Pb collisions at $\sqrt{s_{\text{NN}}} = 5.02\,\text{TeV}$ [15], and in Pb-Pb collisions at $\sqrt{s_{\text{NN}}} = 2.76\,\text{TeV}$ [10]. Vertical bars and boxes represent statistical and systematic uncertainties, respectively. The two lines are theoretical predictions based on two different parameterisations of the source radius.

and ref. [36], respectively. The main difference between the two models concerns the source size R: while in ref. [33] the value of R is constrained from the parameters of a thermal fit, in ref. [36] R is an independent variable, for which the aforementioned p_T dependence has been taken into account. In the former approach, R is about a factor of 2 larger than in the latter, determining very different predictions. The coalescence model predicts a slightly larger yield of triton as compared to helion due to its smaller nuclear radius. In the statistical hadronisation model, the yield ratio between these two nuclei is given by $\exp(-\Delta m/T_{\text{chem}})$, where Δm is the mass difference between triton and helion, taken from ref. [60], and T_{chem} the chemical freeze-out temperature. For the latter, $T_{\text{chem}} = 155\,\text{MeV}$ is used, as done in the canonical statistical model [61]. Given the small mass difference, the statistical hadronisation model predicts a ratio which is very close to unity. The precision of the present data prevents distinguishing between the models. The $^3\text{H}/^3\text{He}$ ratio will be measured with higher precision in Run 3 [62] of the LHC. Indeed, the new ITS, which is characterised by a low material budget, will reduce the systematic uncertainty related to track reconstruction [63]. Moreover, with a better description of the nuclear absorption cross section, it will be possible to reduce the corresponding systematic uncertainties.

4.3 Coalescence parameter as a function of multiplicity

The evolution of B_A with multiplicity $\langle dN_{\text{ch}}/d\eta \rangle$ provides an insight on the dependence of the production mechanisms of light (anti)nuclei. Figure 5(a) shows B_2 as a function of $\langle dN_{\text{ch}}/d\eta \rangle$ for different collision systems and energies at $p_T = 0.75\,\text{GeV}/c$ and B_3 at $p_T = 0.73\,\text{GeV}/c$. The measurements are compared with the theoretical predictions from ref. [58], using $r(\text{d}) = 3.2\,\text{fm}$ and $r(^3\text{He}) = 2.48\,\text{fm}$ as deuteron and helion radii, respectively.

JHEP01(2022)106

Two different parameterisations (named A and B in the following) of the system radius as a function of multiplicity are used. Parameterisation A is based on a fit to the ALICE measurements of system radii R from femtoscopic measurement as a function of multiplicity [64]. In parameterisation B, the relation between the system radius and the multiplicity is fixed to reproduce the B_2 of deuterons in Pb-Pb collisions at $\sqrt{s_{\rm NN}} = 2.76\,\text{TeV}$ in the centrality class 0–10% (see ref. [58] for more details). The B_2 measurement in HM pp collisions agrees with observations in 0-1b collisions at $\sqrt{s_{\rm NN}} = 5\,\text{TeV}$ [15] at similar multiplicity and confirms the trend observed in all the previous measurements. This measurement further strengthen the idea of a production mechanism that depends only on the multiplicity and not on the collision system nor the centre-of-mass energy. Similarly, figure 5(b) shows the evolution of B_3 as a function of multiplicity. The measurements are compared with the theoretical prediction from ref. [58], using the same two paremeterisations as for B_2. Also in this case, the coalescence model qualitatively describes the trend but fails in accurately describing the measurements in the whole multiplicity range. For both B_2 and B_3, one reason could be that multiplicity is not a perfect proxy for the system size, because for each multiplicity the source radius depends also on the transverse momentum of the particle of interest, as shown in figure 2. In the future, it is important to have more measurements of the source radius as a function of $m_{\rm T}$ for the different multiplicity classes in order to test the agreement between the models and the B_A measurement over the whole multiplicity range.

4.4 Ratio between integrated yields of nuclei and protons as a function of multiplicity

The measurements of the ratios between the $p_{\rm T}$-integrated yields of nuclei and protons as a function of multiplicity are shown. Figure 6 shows the measurement for different collision systems and energies for deuterons (d/p) and helions (^{3}He/p), on the left and right panels, respectively. The new measurements complement the existing picture and are consistent with the global trend obtained from previous measurements [10–17], for both d/p and ^{3}He/p: the ratio increases as a function of multiplicity and eventually saturates at high multiplicities. This trend can be interpreted as a consequence of the interplay between the evolution of the yields and of the system size with multiplicity. The measurements are compared with the prediction of both Thermal-FIST Canonical Statistical Model (CSM) [61] and coalescence model [33]. The predictions from CSM suggest correlation volumes $V_{\rm C}$ between 1 and 3 units of rapidity. However, the measurement of the proton-to-pion (p/π) ratio is better described by a correlation volume of 6 rapidity units [28]. On the contrary, the coalescence model provides a better description of the data. For d/p, the agreement is good for the whole multiplicity range. For ^{3}He/p, instead, there are more tensions between data and model in the multiplicity region corresponding to p-Pb and high-multiplicity pp collisions. Remarkably, the two-body coalescence appears to describe the data better than the three-body coalescence prediction.

JHEP01(2022)106

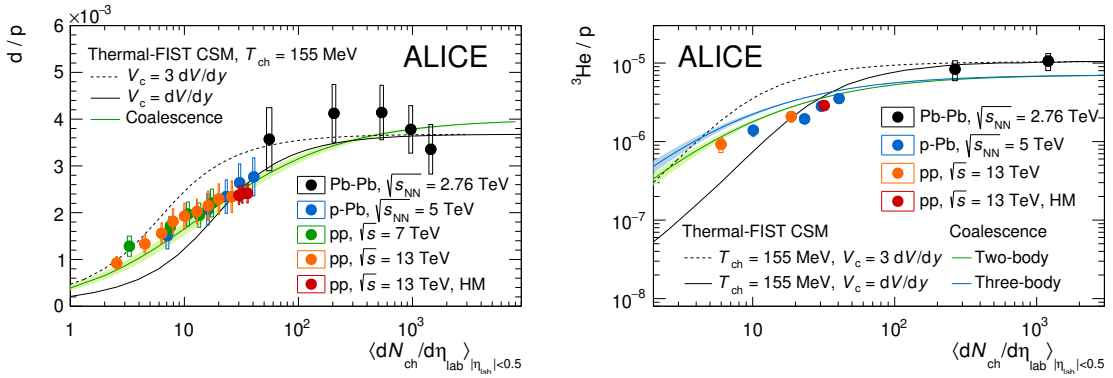

(a) (Anti)deuterons.

(b) (Anti)helions.

Figure 6. Ratio between the p_{T}-integrated yields of nuclei and protons as a function of multiplicity for (anti)deuterons (a) and (anti)helions (b). Measurements are performed in HM pp collisions at $\sqrt{s} = 13\,\mathrm{TeV}$, in MB pp collisions at $\sqrt{s} = 13\,\mathrm{TeV}$ [17] and at $\sqrt{s} = 7\,\mathrm{TeV}$ [11], in p-Pb collisions at $\sqrt{s_{\mathrm{NN}}} = 5.02\,\mathrm{TeV}$ [15, 16], and in Pb-Pb collisions at $\sqrt{s_{\mathrm{NN}}} = 2.76\,\mathrm{TeV}$ [10]. Vertical bars and boxes represent statistical and systematic uncertainties, respectively. The two black lines are the theoretical predictions of the Thermal-FIST CSM [61] for two sizes of the correlation volume V_{C}. For (anti)deuterons, the green line represents the expectation from a coalescence model [33]. For (anti)helion, the blue and green lines represent the expectations from a two-body and three-body coalescence model, respectively [33].

5 Summary

In this paper, the measurements of the production yields of (anti)nuclei in minimum bias and high-multiplicity pp collisions at $\sqrt{s} = 13\,\mathrm{TeV}$ are reported.

A significant increase of the coalescence parameter B_2 with increasing p_{T}/A is observed for the first time in pp collisions. Indeed, previous measurements in small collision systems were consistent with a flat trend within uncertainties. Given the very narrow multiplicity intervals used in the present measurement, this rising trend cannot be attributed to effects coming from a different hardening of the proton and deuteron spectra within the measured multiplicity intervals and thus points to some other physics effect. Moreover, the coalescence parameters are compared with theoretical calculations based on the coalescence approach using different internal wave functions of nuclei. This comparison was possible due to the availability of the measurement of the source radii in the same data sample. While the predictions for B_2 using a Gaussian approximation for the deuteron wave function are in very good agreement with the experimental results, for B_3 they overestimate the data by up to a factor of 2 at the lowest p_{T}. Updated theoretical calculations including also more complex wave functions for ^{3}He would help in providing a better description of this measurement.

The multiplicity evolution of the coalescence parameters for a fixed p_{T}/A and of the ratios of integrated yields d/p and ^{3}He/p are consistent with the global trend from previous measurements. Moreover, the d/p ratio is consistent with predictions from the coalescence model, while significant deviations are observed between the ^{3}He/p and coalescence expec-

JHEP01(2022)106

tations at intermediate multiplicities. The canonical statistical model predictions provide a qualitative description of the particle ratios presented in this paper at low and intermediate multiplicities covered by pp and p-Pb collisions and are consistent with the data only in the grand-canonical limit (multiplicities covered by Pb-Pb collisions).

Acknowledgments

The ALICE Collaboration would like to thank all its engineers and technicians for their invaluable contributions to the construction of the experiment and the CERN accelerator teams for the outstanding performance of the LHC complex. The ALICE Collaboration gratefully acknowledges the resources and support provided by all Grid centres and the Worldwide LHC Computing Grid (WLCG) collaboration. The ALICE Collaboration acknowledges the following funding agencies for their support in building and running the ALICE detector: A. I. Alikhanyan National Science Laboratory (Yerevan Physics Institute) Foundation (ANSL), State Committee of Science and World Federation of Scientists (WFS), Armenia; Austrian Academy of Sciences, Austrian Science Fund (FWF): [M 2467-N36] and Nationalstiftung für Forschung, Technologie und Entwicklung, Austria; Ministry of Communications and High Technologies, National Nuclear Research Center, Azerbaijan; Conselho Nacional de Desenvolvimento Científico e Tecnológico (CNPq), Financiadora de Estudos e Projetos (Finep), Fundação de Amparo à Pesquisa do Estado de São Paulo (FAPESP) and Universidade Federal do Rio Grande do Sul (UFRGS), Brazil; Ministry of Education of China (MOEC) , Ministry of Science & Technology of China (MSTC) and National Natural Science Foundation of China (NSFC), China; Ministry of Science and Education and Croatian Science Foundation, Croatia; Centro de Aplicaciones Tecnológicas y Desarrollo Nuclear (CEADEN), Cubaenergía, Cuba; Ministry of Education, Youth and Sports of the Czech Republic, Czech Republic; The Danish Council for Independent Research | Natural Sciences, the VILLUM FONDEN and Danish National Research Foundation (DNRF), Denmark; Helsinki Institute of Physics (HIP), Finland; Commissariat à l'Energie Atomique (CEA) and Institut National de Physique Nucléaire et de Physique des Particules (IN2P3) and Centre National de la Recherche Scientifique (CNRS), France; Bundesministerium für Bildung und Forschung (BMBF) and GSI Helmholtzzentrum für Schwerionenforschung GmbH, Germany; General Secretariat for Research and Technology, Ministry of Education, Research and Religions, Greece; National Research, Development and Innovation Office, Hungary; Department of Atomic Energy Government of India (DAE), Department of Science and Technology, Government of India (DST), University Grants Commission, Government of India (UGC) and Council of Scientific and Industrial Research (CSIR), India; Indonesian Institute of Science, Indonesia; Istituto Nazionale di Fisica Nucleare (INFN), Italy; Japanese Ministry of Education, Culture, Sports, Science and Technology (MEXT), Japan Society for the Promotion of Science (JSPS) KAKENHI and Japanese Ministry of Education, Culture, Sports, Science and Technology (MEXT)of Applied Science (IIST), Japan; Consejo Nacional de Ciencia (CONACYT) y Tecnología, through Fondo de Cooperación Internacional en Ciencia y Tecnología (FONCICYT) and Dirección General de Asuntos del Personal Academico (DGAPA), Mexico; Nederlandse Or-

ganisatie voor Wetenschappelijk Onderzoek (NWO), Netherlands; The Research Council of Norway, Norway; Commission on Science and Technology for Sustainable Development in the South (COMSATS) and Pakistan Atomic Energy Commission, Pakistan; Pontificia Universidad Católica del Perú, Peru; Ministry of Education and Science, National Science Centre and WUT ID-UB, Poland; Korea Institute of Science and Technology Information and National Research Foundation of Korea (NRF), Republic of Korea; Ministry of Education and Scientific Research, Institute of Atomic Physics and Ministry of Research and Innovation and Institute of Atomic Physics, Romania; Joint Institute for Nuclear Research (JINR), Ministry of Education and Science of the Russian Federation, National Research Centre Kurchatov Institute, Russian Science Foundation and Russian Foundation for Basic Research, Russia; Ministry of Education, Science, Research and Sport of the Slovak Republic, Slovakia; National Research Foundation of South Africa, South Africa; Swedish Research Council (VR) and Knut & Alice Wallenberg Foundation (KAW), Sweden; European Organization for Nuclear Research, Switzerland; Suranaree University of Technology (SUT), National Science and Technology Development Agency (NSDTA) and Office of the Higher Education Commission under NRU project of Thailand, Thailand; Turkish Energy, Nuclear and Mineral Research Agency (TENMAK), Turkey; National Academy of Sciences of Ukraine, Ukraine; Science and Technology Facilities Council (STFC), United Kingdom; National Science Foundation of the United States of America (NSF) and United States Department of Energy, Office of Nuclear Physics (DOE NP), United States of America. In addition, individual groups and members have received support from European Research Council, European Union.

JHEP01(2022)106

A Theoretical prediction for the coalescence parameter B_A

In this appendix, the details about the theoretical prediction used for the coalescence parameter B_A as a function of the source radius are reported. The general recipe is taken from ref. [36]. B_2 is defined as

$$B_2(p) \approx \frac{3}{2m} \int \mathrm{d}^3q \, D(\vec{q}) \, \mathcal{C}_2^{\mathrm{PRF}}(\vec{p}, \vec{q}) \,, \tag{A.1}$$

where m is the proton mass, p is the momentum of the nucleus, q is the relative momentum of the nucleons, $D(\vec{q})$ is the deuteron Wigner density and $\mathcal{C}_2^{\mathrm{PRF}}(\vec{p}, \vec{q})$ is the correlation between two nucleons in the rest frame of the pair (PRF), assuming a Gaussian source model. For these calculations, we assume a homogeneous source, i.e. $R = R_{\parallel} = R_{\perp}$. Hence, the correlation function has the form

$$\mathcal{C}_2^{\mathrm{PRF}}(\vec{p}, \vec{q}) = e^{-R^2 q^2}, \tag{A.2}$$

where R is the source radius. Finally, the Wigner density is defined as

$$D(\vec{q}) = \int \mathrm{d}^3r \, |\phi_{\mathrm{d}}(\vec{r})|^2 e^{-i\vec{q}\cdot\vec{r}}, \tag{A.3}$$

where ϕ_{d} is the deuteron wave function. In the following, we will provide different predictions for B_2 as a function of the source radius R starting from eq. (A.1) and using different

wave functions $\phi_{\rm d}$. The theoretical predictions for B_2 as a function of the source radius R is shown in figure 7(a). At large values of the source radius they all show the same trend. On the contrary, for small values they differ, with a maximum spread of around a factor of 10. Eq. (A.1) has not an equivalent for B_3 and *ab initio* calculations are needed. For this reason, it is currently not possible to obtain B_3 predictions for different wave functions as easily as for B_2. However, it is possible to obtain a prediction for the case of a simple Gaussian wave function (see eq. (A.7)).

A.1 Gaussian wave function

The most simple assumption is a Gaussian wave function

$$\phi_{\rm d}(r) = \frac{e^{-\frac{r^2}{2d^2}}}{(\pi d^2)^{3/4}}, \tag{A.4}$$

where d is the nucleus radius. For this calculations, $d = 3.2\,\text{fm}$, as in ref. [36]. The corresponding Wigner density is

$$D(\vec{q}) = e^{-\frac{q^2 d^2}{4}}. \tag{A.5}$$

This brings to the expression for B_2 as a function of the source radius R

$$B_2(R) = \frac{3\pi^2}{2m\left[R^2 + \left(\frac{d}{2}\right)^2\right]^{\frac{3}{2}}}. \tag{A.6}$$

This function is shown in figure 7(a), together with the other predictions for B_2. As shown in ref. [36], eq. (A.6) can also be generalised for a nucleus with mass number A

$$B_A(R) = \frac{2J_A+1}{2^A\sqrt{A}}\frac{1}{m^{A-1}}\left[\frac{2\pi}{R^2 + (r_A/2)^2}\right]^{\frac{3}{2}(A-1)}, \tag{A.7}$$

where J_A is the spin of the nucleus. Eq. (A.7) is used to calculate the theoretical prediction for B_3, shown in figure 7(b).

A.2 Hulthen wave function

The second hypothesis tested here is a Hulthen wave function

$$\phi_{\rm d}(r) = \sqrt{\frac{\alpha\beta(\alpha+\beta)}{2\pi(\alpha-\beta)^2}}\,\frac{e^{-\alpha r} - e^{-\beta r}}{r}, \tag{A.8}$$

where $\alpha = 0.2$ fm^{-1} and $\beta = 1.56$ fm^{-1} are parameters taken from ref. [32]. The corresponding expression for B_2 is

$$B_2(R) = \frac{3\pi^2}{R^2}\frac{\alpha\beta(\alpha+\beta)}{(\alpha-\beta)^2}\left[e^{4\alpha^2R^2}\text{erfc}(2\alpha R) - 2e^{(\alpha+\beta)^2R^2}\text{erfc}((\alpha+\beta)R) + e^{4\beta^2R^2}\text{erfc}(2\beta R)\right]. \tag{A.9}$$

This function is shown in figure 7(a), together with the other predictions for B_2.

JHEP01(2022)106

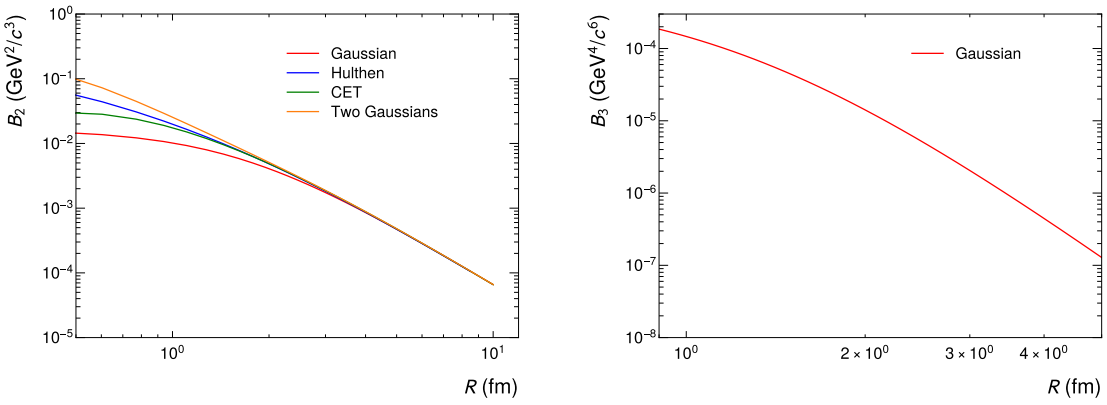

(a) (b)

Figure 7. Coalescence parameters B_2 (a) and B_3 (b) as a function of the source radius R for different wave functions (see the text for more details).

A.3 Chiral Effective Field Theory wave function

The third hypothesis for deuteron wave function is obtained from Chiral Effective field theory (χEFT) calculations (N^{4}LO). It is based on ref. [57] and the normalisation is based on ref. [65]. A cutoff at $\Lambda_c = 500\,\text{MeV}$ is used. The deuteron wave function is

$$\phi_{\text{d}}(\vec{r}) = \frac{1}{\sqrt{4\pi}\,r}\left[u(r) \,+\, \frac{1}{\sqrt{8}}\,w(r)\,S_{12}(\hat{r})\right]\,\chi_{1m}\,, \tag{A.10}$$

where $u(r)$ and $w(r)$ are radial wave functions, $S_{12}(\hat{r})$ is the spin tensor and χ_{1m} is a spinor. The spin-averaged density of the deuteron can be hence expressed as

$$|\phi_{\text{d}}(r)|^2 = \frac{1}{4\pi\,r^2}\left[u^2(r) \,+\, w^2(r)\right]. \tag{A.11}$$

Using eq. (A.1) and eq. (A.3), one obtains

$$B_2(R) = \frac{6\pi}{m}\int_0^{\Lambda_c} \text{d}q \int_0^{\infty} \text{d}r\, q\,\left[u(r)^2 \,+\, w(r)^2\right]\,\frac{\sin(qr)}{r}\,e^{-R^2q^2}. \tag{A.12}$$

Integrating eq. (A.12) over q, one obtains

$$\begin{aligned} B_2(R) = \frac{3\pi}{mR^2}\int_0^{\infty}\frac{\text{d}r}{r}\,\left[u^2(r) \,+\, w^2(r)\right]\,\Bigg\{ & e^{-\Lambda_c^2R^2}\sin(\Lambda_c r) \\ & +\, \frac{\sqrt{\pi}r}{4R}\,e^{-\frac{r^2}{4R^2}}\left[\text{erf}\left(\frac{ir+2R^2\Lambda_c}{2R}\right) \,-\, \text{erf}\left(\frac{ir-2R^2\Lambda_c}{2R}\right)\right]\Bigg\}. \end{aligned} \tag{A.13}$$

This function is shown in figure 7(a), together with the other predictions for B_2.

A.4 Combination of two Gaussians

The last considered wave function is a combination of two Gaussians, fitted to the Hulthen wave function [34]:

$$\phi_{\text{d}}(r) = \pi^{-3/4}\left[\frac{\Delta^{1/2}}{d_1^{3/2}}e^{-r^2/(2d_1^2)} \,+\, e^{i\alpha}\frac{(1-\Delta)^{1/2}}{d_2^{3/2}}e^{-r^2/(2d_2^2)}\right] \tag{A.14}$$

JHEP01(2022)106

where $\Delta = 0.581$, $d_1 = 3.979\,\text{fm}$ and $d_1 = 0.890\,\text{fm}$. The corresponding density is

$$|\phi_{\text{d}}(r)|^2 = \pi^{-3/2}\left[\frac{\Delta}{d_1^3}e^{-r^2/d_1^2} + \frac{1-\Delta}{d_2^3}e^{-r^2/d_2^2}\right]. \tag{A.15}$$

B_2 can be hence written as

$$B_2(R) = \frac{24\pi^{5/2}}{m}\int_0^\infty \text{d}q \int_0^\infty \text{d}r\,|\phi_d(r)|^2 \sin(qr)\, r\, q\, e^{-R^2q^2}, \tag{A.16}$$

and after integrating over q and r, one obtains:

$$B_2(R) = \frac{3\pi^{3/2}}{2mR^3}\left[\Delta\left(1 + \frac{d_1^2}{4R^2}\right)^{-3/2} + (1-\Delta)\left(1 + \frac{d_2^2}{4R^2}\right)^{-3/2}\right]. \tag{A.17}$$

This function is shown in figure 7(a), together with the other predictions for B_2.

References

[1] ALICE collaboration, ${}^{3}_{\Lambda}\text{H}$ *and* ${}^{3}_{\Lambda}\overline{\text{H}}$ *production in Pb-Pb collisions at* $\sqrt{s_{\text{NN}}} = 2.76$ *TeV*, *Phys. Lett. B* **754** (2016) 360 [arXiv:1506.08453] [INSPIRE].

[2] V.T. Cocconi, T. Fazzini, G. Fidecaro, M. Legros, N.H. Lipman and A.W. Merrison, *Mass analysis of the secondary particles produced by the* 25 *GeV proton beam of the CERN proton synchrotron*, *Phys. Rev. Lett.* **5** (1960) 19 [INSPIRE].

[3] S. Nagamiya, *Experimental overview*, *Nucl. Phys. A* **544** (1992) 5.

[4] STAR collaboration, *Anti-deuteron and anti-*^{3}*He production in* $\sqrt{s_{\text{NN}}} = 130$ *GeV Au+Au collisions*, *Phys. Rev. Lett.* **87** (2001) 262301 [*Erratum ibid.* **87** (2001) 279902] [nucl-ex/0108022] [INSPIRE].

[5] PHENIX collaboration, *Deuteron and antideuteron production in Au + Au collisions at* $\sqrt{s_{\text{NN}}} = 200$ *GeV*, *Phys. Rev. Lett.* **94** (2005) 122302 [nucl-ex/0406004] [INSPIRE].

[6] BRAHMS collaboration, *Rapidity dependence of deuteron production in Au+Au collisions at* $\sqrt{s_{\text{NN}}} = 200$ *GeV*, *Phys. Rev. C* **83** (2011) 044906 [arXiv:1005.5427] [INSPIRE].

[7] STAR collaboration, *Beam energy dependence of d and* $\bar{d}$ *productions in Au+Au collisions at RHIC*, *Nucl. Phys. A* **967** (2017) 788 [arXiv:1704.04335] [INSPIRE].

[8] STAR collaboration, *Observation of an antimatter hypernucleus*, *Science* **328** (2010) 58 [arXiv:1003.2030] [INSPIRE].

[9] STAR collaboration, *Observation of the antimatter helium-4 nucleus*, *Nature* **473** (2011) 353 [*Erratum ibid.* **475** (2011) 412] [arXiv:1103.3312] [INSPIRE].

[10] ALICE collaboration, *Production of light nuclei and anti-nuclei in pp and Pb-Pb collisions at energies available at the CERN Large Hadron Collider*, *Phys. Rev. C* **93** (2016) 024917 [arXiv:1506.08951] [INSPIRE].

JHEP01(2022)106

[11] ALICE collaboration, *Multiplicity dependence of (anti-)deuteron production in pp collisions at* $\sqrt{s} = 7$ *TeV*, *Phys. Lett. B* **794** (2019) 50 [arXiv:1902.09290] [INSPIRE].

[12] ALICE collaboration, *Measurement of deuteron spectra and elliptic flow in Pb-Pb collisions at* $\sqrt{s_{\rm NN}} = 2.76$ *TeV at the LHC*, *Eur. Phys. J. C* **77** (2017) 658 [arXiv:1707.07304] [INSPIRE].

[13] ALICE collaboration, *Production of deuterons, tritons,* ^{3}*He nuclei and their antinuclei in pp collisions at* $\sqrt{s} = 0.9$*,* 2.76 *and* 7 *TeV*, *Phys. Rev. C* **97** (2018) 024615 [arXiv:1709.08522] [INSPIRE].

[14] ALICE collaboration, *Production of* ^{4}*He and* $^4\overline{He}$ *in Pb-Pb collisions at* $\sqrt{s_{\rm NN}} = 2.76$ *TeV at the LHC*, *Nucl. Phys. A* **971** (2018) 1 [arXiv:1710.07531] [INSPIRE].

[15] ALICE collaboration, *Multiplicity dependence of light (anti-)nuclei production in p-Pb collisions at* $\sqrt{s_{\rm NN}} = 5.02$ *TeV*, *Phys. Lett. B* **800** (2020) 135043 [arXiv:1906.03136] [INSPIRE].

[16] ALICE collaboration, *Production of (anti-)*^{3}*He and (anti-)*^{3}*H in p-Pb collisions at* $\sqrt{s_{\rm NN}} = 5.02$ *TeV*, *Phys. Rev. C* **101** (2020) 044906 [arXiv:1910.14401] [INSPIRE].

[17] ALICE collaboration, *(Anti-)deuteron production in pp collisions at* $\sqrt{s} = 13$ *TeV*, *Eur. Phys. J. C* **80** (2020) 889 [arXiv:2003.03184] [INSPIRE].

[18] K. Blum, K.C.Y. Ng, R. Sato and M. Takimoto, *Cosmic rays, antihelium, and an old navy spotlight*, *Phys. Rev. D* **96** (2017) 103021 [arXiv:1704.05431] [INSPIRE].

[19] V. Poulin, P. Salati, I. Cholis, M. Kamionkowski and J. Silk, *Where do the AMS-02 antihelium events come from?*, *Phys. Rev. D* **99** (2019) 023016 [arXiv:1808.08961] [INSPIRE].

[20] M. Korsmeier, F. Donato and N. Fornengo, *Prospects to verify a possible dark matter hint in cosmic antiprotons with antideuterons and antihelium*, *Phys. Rev. D* **97** (2018) 103011 [arXiv:1711.08465] [INSPIRE].

[21] Y. Cui, J.D. Mason and L. Randall, *General analysis of antideuteron searches for dark matter*, *JHEP* **11** (2010) 017 [arXiv:1006.0983] [INSPIRE].

[22] J. Cleymans, S. Kabana, I. Kraus, H. Oeschler, K. Redlich and N. Sharma, *Antimatter production in proton-proton and heavy-ion collisions at ultrarelativistic energies*, *Phys. Rev. C* **84** (2011) 054916 [arXiv:1105.3719] [INSPIRE].

[23] A. Andronic, P. Braun-Munzinger, J. Stachel and H. Stocker, *Production of light nuclei, hypernuclei and their antiparticles in relativistic nuclear collisions*, *Phys. Lett. B* **697** (2011) 203 [arXiv:1010.2995] [INSPIRE].

[24] F. Becattini, E. Grossi, M. Bleicher, J. Steinheimer and R. Stock, *Centrality dependence of hadronization and chemical freeze-out conditions in heavy ion collisions at* $\sqrt{s_{\rm NN}} = 2.76$ *TeV*, *Phys. Rev. C* **90** (2014) 054907 [arXiv:1405.0710] [INSPIRE].

[25] V. Vovchenko and H. Stoecker, *Examination of the sensitivity of the thermal fits to heavy-ion hadron yield data to the modeling of the eigenvolume interactions*, *Phys. Rev. C* **95** (2017) 044904 [arXiv:1606.06218] [INSPIRE].

[26] A. Andronic, P. Braun-Munzinger, K. Redlich and J. Stachel, *Decoding the phase structure of QCD via particle production at high energy*, *Nature* **561** (2018) 321 [arXiv:1710.09425] [INSPIRE].

JHEP01(2022)106

[27] N. Sharma, J. Cleymans, B. Hippolyte and M. Paradza, *A comparison of p-p, p-Pb, Pb-Pb collisions in the thermal model: multiplicity dependence of thermal parameters*, *Phys. Rev. C* **99** (2019) 044914 [arXiv:1811.00399] [INSPIRE].

[28] V. Vovchenko, B. Dönigus and H. Stoecker, *Canonical statistical model analysis of p-p , p-Pb, and Pb-Pb collisions at energies available at the CERN Large Hadron Collider*, *Phys. Rev. C* **100** (2019) 054906 [arXiv:1906.03145] [INSPIRE].

[29] S.T. Butler and C.A. Pearson, *Deuterons from high-energy proton bombardment of matter*, *Phys. Rev.* **129** (1963) 836 [INSPIRE].

[30] J.I. Kapusta, *Mechanisms for deuteron production in relativistic nuclear collisions*, *Phys. Rev. C* **21** (1980) 1301 [INSPIRE].

[31] W. Zhao, L. Zhu, H. Zheng, C.M. Ko and H. Song, *Spectra and flow of light nuclei in relativistic heavy ion collisions at energies available at the BNL Relativistic Heavy Ion Collider and at the CERN Large Hadron Collider*, *Phys. Rev. C* **98** (2018) 054905 [arXiv:1807.02813] [INSPIRE].

[32] R. Scheibl and U.W. Heinz, *Coalescence and flow in ultrarelativistic heavy ion collisions*, *Phys. Rev. C* **59** (1999) 1585 [nucl-th/9809092] [INSPIRE].

[33] K.-J. Sun, C.M. Ko and B. Dönigus, *Suppression of light nuclei production in collisions of small systems at the Large Hadron Collider*, *Phys. Lett. B* **792** (2019) 132 [arXiv:1812.05175] [INSPIRE].

[34] M. Kachelrieß, S. Ostapchenko and J. Tjemsland, *Alternative coalescence model for deuteron, tritium, helium-3 and their antinuclei*, *Eur. Phys. J. A* **56** (2020) 4 [arXiv:1905.01192] [INSPIRE].

[35] ALICE collaboration, *Jet-associated deuteron production in pp collisions at* $\sqrt{s} = 13$ *TeV*, *Phys. Lett. B* **819** (2021) 136440 [arXiv:2011.05898] [INSPIRE].

[36] K. Blum and M. Takimoto, *Nuclear coalescence from correlation functions*, *Phys. Rev. C* **99** (2019) 044913 [arXiv:1901.07088] [INSPIRE].

[37] ALICE collaboration, *Search for a common baryon source in high-multiplicity pp collisions at the LHC*, *Phys. Lett. B* **811** (2020) 135849 [arXiv:2004.08018] [INSPIRE].

[38] ALICE collaboration, *The ALICE experiment at the CERN LHC*, 2008 *JINST* **3** S08002 [INSPIRE].

[39] ALICE collaboration, *Performance of the ALICE experiment at the CERN LHC*, *Int. J. Mod. Phys. A* **29** (2014) 1430044 [arXiv:1402.4476] [INSPIRE].

[40] ALICE collaboration, *Alignment of the ALICE inner tracking system with cosmic-ray tracks*, 2010 *JINST* **5** P03003 [arXiv:1001.0502] [INSPIRE].

[41] J. Alme et al., *The ALICE TPC, a large 3-dimensional tracking device with fast readout for ultra-high multiplicity events*, *Nucl. Instrum. Meth. A* **622** (2010) 316 [arXiv:1001.1950] [INSPIRE].

[42] A. Akindinov et al., *Performance of the ALICE time-of-flight detector at the LHC*, *Eur. Phys. J. Plus* **128** (2013) 44 [INSPIRE].

[43] ALICE collaboration, *Performance of the ALICE VZERO system*, 2013 *JINST* **8** P10016 [arXiv:1306.3130] [INSPIRE].

JHEP01(2022)106

[44] ALICE collaboration, *Multiplicity dependence of light-flavor hadron production in pp collisions at* $\sqrt{s} = 7$ *TeV*, *Phys. Rev. C* **99** (2019) 024906 [arXiv:1807.11321] [INSPIRE].

[45] ALICE collaboration, *Multiplicity dependence of (multi-)strange hadron production in proton-proton collisions at* $\sqrt{s} = 13$ *TeV*, *Eur. Phys. J. C* **80** (2020) 167 [arXiv:1908.01861] [INSPIRE].

[46] ALICE collaboration, *Pseudorapidity density of charged particles in p+Pb collisions at* $\sqrt{s_{\rm NN}} = 5.02$ *TeV*, *Phys. Rev. Lett.* **110** (2013) 032301 [arXiv:1210.3615] [INSPIRE].

[47] T. Sjöstrand, S. Mrenna and P.Z. Skands, *A brief introduction to PYTHIA* 8.1, *Comput. Phys. Commun.* **178** (2008) 852 [arXiv:0710.3820] [INSPIRE].

[48] P. Skands, S. Carrazza and J. Rojo, *Tuning PYTHIA* 8.1*: the Monash* 2013 *tune*, *Eur. Phys. J. C* **74** (2014) 3024 [arXiv:1404.5630] [INSPIRE].

[49] GEANT4 collaboration, *GEANT4 — a simulation toolkit*, *Nucl. Instrum. Meth. A* **506** (2003) 250 [INSPIRE].

[50] ALICE collaboration, *Measurement of the low-energy antideuteron inelastic cross section*, *Phys. Rev. Lett.* **125** (2020) 162001 [arXiv:2005.11122] [INSPIRE].

[51] R. Brun et al., *GEANT: detector description and simulation tool*, CERN-W5013, CERN, Geneva, Switzerland (2008).

[52] C. Tsallis, *Possible generalization of Boltzmann-Gibbs statistics*, *J. Statist. Phys.* **52** (1988) 479 [INSPIRE].

[53] E. Schnedermann, J. Sollfrank and U.W. Heinz, *Thermal phenomenology of hadrons from* 200-*A/GeV S+S collisions*, *Phys. Rev. C* **48** (1993) 2462 [nucl-th/9307020] [INSPIRE].

[54] STAR collaboration, *Identified particle elliptic flow in Au+Au collisions at* $\sqrt{s_{\rm NN}} = 130$ *GeV*, *Phys. Rev. Lett.* **87** (2001) 182301 [nucl-ex/0107003] [INSPIRE].

[55] P.J. Siemens and J.O. Rasmussen, *Evidence for a blast wave from compress nuclear matter*, *Phys. Rev. Lett.* **42** (1979) 880 [INSPIRE].

[56] F. Bellini, K. Blum, A.P. Kalweit and M. Puccio, *Examination of coalescence as the origin of nuclei in hadronic collisions*, *Phys. Rev. C* **103** (2021) 014907 [arXiv:2007.01750] [INSPIRE].

[57] D.R. Entem, R. Machleidt and Y. Nosyk, *High-quality two-nucleon potentials up to fifth order of the chiral expansion*, *Phys. Rev. C* **96** (2017) 024004 [arXiv:1703.05454] [INSPIRE].

[58] F. Bellini and A.P. Kalweit, *Testing production scenarios for (anti-)(hyper-)nuclei and exotica at energies available at the CERN Large Hadron Collider*, *Phys. Rev. C* **99** (2019) 054905 [arXiv:1807.05894] [INSPIRE].

[59] R.J.N. Phillips, *The two-nucleon interaction*, *Repts. Prog. Phys.* **22** (1959) 562.

[60] E. Tiesinga, P.J. Mohr, D.B. Newell and B.N. Taylor, *CODATA recommended values of the fundamental physical constants:* 2018, *Rev. Mod. Phys.* **93** (2021) 025010 [INSPIRE].

[61] V. Vovchenko, B. Dönigus and H. Stoecker, *Multiplicity dependence of light nuclei production at LHC energies in the canonical statistical model*, *Phys. Lett. B* **785** (2018) 171 [arXiv:1808.05245] [INSPIRE].

[62] ALICE collaboration, *Future high-energy pp programme with ALICE*, ALICE-PUBLIC-2020-005, CERN, Geneva, Switzerland (2020).

JHEP01(2022)106

[63] ALICE collaboration, *Technical design report for the upgrade of the ALICE inner tracking system*, *J. Phys. G* **41** (2014) 087002 [INSPIRE].

[64] ALICE collaboration, *Charged kaon femtoscopic correlations in pp collisions at* $\sqrt{s} = 7$ *TeV*, *Phys. Rev. D* **87** (2013) 052016 [arXiv:1212.5958] [INSPIRE].

[65] R. Machleidt, *The high precision, charge dependent Bonn nucleon-nucleon potential (CD-Bonn)*, *Phys. Rev. C* **63** (2001) 024001 [nucl-th/0006014] [INSPIRE].

JHEP01(2022)106

The ALICE collaboration

S. Acharya[144], D. Adamová[98], A. Adler[76], J. Adolfsson[83], G. Aglieri Rinella[35], M. Agnello[31], N. Agrawal[55], Z. Ahammed[144], S. Ahmad[16], S.U. Ahn[78], I. Ahuja[39], Z. Akbar[52], A. Akindinov[95], M. Al-Turany[111], S.N. Alam[16,41], D. Aleksandrov[91], B. Alessandro[61], H.M. Alfanda[7], R. Alfaro Molina[73], B. Ali[16], Y. Ali[14], A. Alici[26], N. Alizadehvandchali[128], A. Alkin[35], J. Alme[21], T. Alt[70], L. Altenkamper[21], I. Altsybeev[116], M.N. Anaam[7], C. Andrei[49], D. Andreou[93], A. Andronic[147], M. Angeletti[35], V. Anguelov[107], F. Antinori[58], P. Antonioli[55], C. Anuj[16], N. Apadula[82], L. Aphecetche[118], H. Appelshäuser[70], S. Arcelli[26], R. Arnaldi[61], I.C. Arsene[20], M. Arslandok[149,107], A. Augustinus[35], R. Averbeck[111], S. Aziz[80], M.D. Azmi[16], A. Badalà[57], Y.W. Baek[42], X. Bai[132,111], R. Bailhache[70], Y. Bailung[51], R. Bala[104], A. Balbino[31], A. Baldisseri[141], B. Balis[2], D. Banerjee[4], R. Barbera[27], L. Barioglio[108], M. Barlou[87], G.G. Barnaföldi[148], L.S. Barnby[97], V. Barret[138], C. Bartels[131], K. Barth[35], E. Bartsch[70], F. Baruffaldi[28], N. Bastid[138], S. Basu[83], G. Batigne[118], B. Batyunya[77], D. Bauri[50], J.L. Bazo Alba[115], I.G. Bearden[92], C. Beattie[149], I. Belikov[140], A.D.C. Bell Hechavarria[147], F. Bellini[26], R. Bellwied[128], S. Belokurova[116], V. Belyaev[96], G. Bencedi[148,71], S. Beole[25], A. Bercuci[49], Y. Berdnikov[101], A. Berdnikova[107], L. Bergmann[107], M.G. Besoiu[69], L. Betev[35], P.P. Bhaduri[144], A. Bhasin[104], I.R. Bhat[104], M.A. Bhat[4], B. Bhattacharjee[43], P. Bhattacharya[23], L. Bianchi[25], N. Bianchi[53], J. Bielčík[38], J. Bielčíková[98], J. Biernat[121], A. Bilandzic[108], G. Biro[148], S. Biswas[4], J.T. Blair[122], D. Blau[91,84], M.B. Blidaru[111], C. Blume[70], G. Boca[29,59], F. Bock[99], A. Bogdanov[96], S. Boi[23], J. Bok[63], L. Boldizsár[148], A. Bolozdynya[96], M. Bombara[39], P.M. Bond[35], G. Bonomi[143,59], H. Borel[141], A. Borissov[84], H. Bossi[149], E. Botta[25], L. Bratrud[70], P. Braun-Munzinger[111], M. Bregant[124], M. Broz[38], G.E. Bruno[110,34], M.D. Buckland[131], D. Budnikov[112], H. Buesching[70], S. Bufalino[31], O. Bugnon[118], P. Buhler[117], Z. Buthelezi[74,135], J.B. Butt[14], A. Bylinkin[130], S.A. Bysiak[121], M. Cai[28,7], H. Caines[149], A. Caliva[111], E. Calvo Villar[115], J.M.M. Camacho[123], R.S. Camacho[46], P. Camerini[24], F.D.M. Canedo[124], F. Carnesecchi[35,26], R. Caron[141], J. Castillo Castellanos[141], E.A.R. Casula[23], F. Catalano[31], C. Ceballos Sanchez[77], P. Chakraborty[50], S. Chandra[144], S. Chapeland[35], M. Chartier[131], S. Chattopadhyay[144], S. Chattopadhyay[113], A. Chauvin[23], T.G. Chavez[46], T. Cheng[7], C. Cheshkov[139], B. Cheynis[139], V. Chibante Barroso[35], D.D. Chinellato[125], S. Cho[63], P. Chochula[35], P. Christakoglou[93], C.H. Christensen[92], P. Christiansen[83], T. Chujo[137], C. Cicalo[56], L. Cifarelli[26], F. Cindolo[55], M.R. Ciupek[111], G. Clai[II,55], J. Cleymans[I,127], F. Colamaria[54], J.S. Colburn[114], D. Colella[110,54,34,148], A. Collu[82], M. Colocci[35], M. Concas[III,61], G. Conesa Balbastre[81], Z. Conesa del Valle[80], G. Contin[24], J.G. Contreras[38], M.L. Coquet[141], T.M. Cormier[99], P. Cortese[32], M.R. Cosentino[126], F. Costa[35], S. Costanza[29,59], P. Crochet[138], R. Cruz-Torres[82], E. Cuautle[71], P. Cui[7], L. Cunqueiro[99], A. Dainese[58], M.C. Danisch[107], A. Danu[69], I. Das[113], P. Das[89], P. Das[4], S. Das[4], S. Dash[50], S. De[89], A. De Caro[30], G. de Cataldo[54], L. De Cilladi[25], J. de Cuveland[40], A. De Falco[23], D. De Gruttola[30], N. De Marco[61], C. De Martin[24], S. De Pasquale[30], S. Deb[51], H.F. Degenhardt[124], K.R. Deja[145], L. Dello Stritto[30], W. Deng[7], P. Dhankher[19], D. Di Bari[34], A. Di Mauro[35], R.A. Diaz[8], T. Dietel[127], Y. Ding[139,7], R. Divià[35], D.U. Dixit[19], Ø. Djuvsland[21], U. Dmitrieva[65], J. Do[63], A. Dobrin[69], B. Dönigus[70], O. Dordic[20], A.K. Dubey[144], A. Dubla[111,93], S. Dudi[103], M. Dukhishyam[89], P. Dupieux[138], N. Dzalaiova[13], T.M. Eder[147], R.J. Ehlers[99], V.N. Eikeland[21], F. Eisenhut[70], D. Elia[54], B. Erazmus[118], F. Ercolessi[26], F. Erhardt[102], A. Erokhin[116], M.R. Ersdal[21], B. Espagnon[80], G. Eulisse[35], D. Evans[114], S. Evdokimov[94], L. Fabbietti[108], M. Faggin[28], J. Faivre[81], F. Fan[7], A. Fantoni[53], M. Fasel[99], P. Fecchio[31], A. Feliciello[61], G. Feofilov[116], A. Fernández Téllez[46], A. Ferrero[141], A. Ferretti[25], V.J.G. Feuillard[107], J. Figiel[121], S. Filchagin[112], D. Finogeev[65], F.M. Fionda[56,21], G. Fiorenza[35,110], F. Flor[128], A.N. Flores[122], S. Foertsch[74], P. Foka[111],

JHEP01(2022)106

S. Fokin[91], E. Fragiacomo[62], E. Frajna[148], U. Fuchs[35], N. Funicello[30], C. Furget[81], A. Furs[65], J.J. Gaardhøje[92], M. Gagliardi[25], A.M. Gago[115], A. Gal[140], C.D. Galvan[123], P. Ganoti[87], C. Garabatos[111], J.R.A. Garcia[46], E. Garcia-Solis[10], K. Garg[118], C. Gargiulo[35], A. Garibli[90], K. Garner[147], P. Gasik[111], E.F. Gauger[122], A. Gautam[130], M.B. Gay Ducati[72], M. Germain[118], P. Ghosh[144], S.K. Ghosh[4], M. Giacalone[26], P. Gianotti[53], P. Giubellino[111,61], P. Giubilato[28], A.M.C. Glaenzer[141], P. Glässel[107], D.J.Q. Goh[85], V. Gonzalez[146], L.H. González-Trueba[73], S. Gorbunov[40], M. Gorgon[2], L. Görlich[121], S. Gotovac[36], V. Grabski[73], L.K. Graczykowski[145], L. Greiner[82], A. Grelli[64], C. Grigoras[35], V. Grigoriev[96], S. Grigoryan[77,1], F. Grosa[35,61], J.F. Grosse-Oetringhaus[35], R. Grosso[111], G.G. Guardiano[125], R. Guernane[81], M. Guilbaud[118], K. Gulbrandsen[92], T. Gunji[136], W. Guo[7], A. Gupta[104], R. Gupta[104], S.P. Guzman[46], L. Gyulai[148], M.K. Habib[111], C. Hadjidakis[80], G. Halimoglu[70], H. Hamagaki[85], M. Hamid[7], R. Hannigan[122], M.R. Haque[145,89], A. Harlenderova[111], J.W. Harris[149], A. Harton[10], J.A. Hasenbichler[35], H. Hassan[99], D. Hatzifotiadou[55], P. Hauer[44], L.B. Havener[149], S.T. Heckel[108], E. Hellbär[111], H. Helstrup[37], T. Herman[38], E.G. Hernandez[46], G. Herrera Corral[9], F. Herrmann[147], K.F. Hetland[37], H. Hillemanns[35], C. Hills[131], B. Hippolyte[140], B. Hofman[64], B. Hohlweger[93], J. Honermann[147], G.H. Hong[150], D. Horak[38], S. Hornung[111], A. Horzyk[2], R. Hosokawa[15], Y. Hou[7], P. Hristov[35], C. Hughes[134], P. Huhn[70], L.M. Huhta[129], T.J. Humanic[100], H. Hushnud[113], L.A. Husova[147], A. Hutson[128], D. Hutter[40], J.P. Iddon[35,131], R. Ilkaev[112], H. Ilyas[14], M. Inaba[137], G.M. Innocenti[35], M. Ippolitov[91], A. Isakov[38,98], M.S. Islam[113], M. Ivanov[111], V. Ivanov[101], V. Izucheev[94], M. Jablonski[2], B. Jacak[82], N. Jacazio[35], P.M. Jacobs[82], S. Jadlovska[120], J. Jadlovsky[120], S. Jaelani[64], C. Jahnke[125,124], M.J. Jakubowska[145], A. Jalotra[104], M.A. Janik[145], T. Janson[76], M. Jercic[102], O. Jevons[114], A.A.P. Jimenez[71], F. Jonas[99,147], P.G. Jones[114], J.M. Jowett [35,111], J. Jung[70], M. Jung[70], A. Junique[35], A. Jusko[114], J. Kaewjai[119], P. Kalinak[66], A.S. Kalteyer[111], A. Kalweit[35], V. Kaplin[96], A. Karasu Uysal[79], D. Karatovic[102], O. Karavichev[65], T. Karavicheva[65], P. Karczmarczyk[145], E. Karpechev[65], A. Kazantsev[91], U. Kebschull[76], R. Keidel[48], D.L.D. Keijdener[64], M. Keil[35], B. Ketzer[44], Z. Khabanova[93], A.M. Khan[7], S. Khan[16], A. Khanzadeev[101], Y. Kharlov[94,84], A. Khatun[16], A. Khuntia[121], B. Kileng[37], B. Kim[17,63], C. Kim[17], D.J. Kim[129], E.J. Kim[75], J. Kim[150], J.S. Kim[42], J. Kim[107], J. Kim[150], J. Kim[75], M. Kim[107], S. Kim[18], T. Kim[150], S. Kirsch[70], I. Kisel[40], S. Kiselev[95], A. Kisiel[145], J.P. Kitowski[2], J.L. Klay[6], J. Klein[35], S. Klein[82], C. Klein-Bösing[147], M. Kleiner[70], T. Klemenz[108], A. Kluge[35], A.G. Knospe[128], C. Kobdaj[119], M.K. Köhler[107], T. Kollegger[111], A. Kondratyev[77], N. Kondratyeva[96], E. Kondratyuk[94], J. Konig[70], S.A. Konigstorfer[108], P.J. Konopka[35], G. Kornakov[145], S.D. Koryciak[2], A. Kotliarov[98], O. Kovalenko[88], V. Kovalenko[116], M. Kowalski[121], I. Králik[66], A. Kravčáková[39], L. Kreis[111], M. Krivda[114,66], F. Krizek[98], K. Krizkova Gajdosova[38], M. Kroesen[107], M. Krüger[70], E. Kryshen[101], M. Krzewicki[40], V. Kučera[35], C. Kuhn[140], P.G. Kuijer[93], T. Kumaoka[137], D. Kumar[144], L. Kumar[103], N. Kumar[103], S. Kundu[35], P. Kurashvili[88], A. Kurepin[65], A.B. Kurepin[65], A. Kuryakin[112], S. Kushpil[98], J. Kvapil[114], M.J. Kweon[63], J.Y. Kwon[63], Y. Kwon[150], S.L. La Pointe[40], P. La Rocca[27], Y.S. Lai[82], A. Lakrathok[119], M. Lamanna[35], R. Langoy[133], K. Lapidus[35], P. Larionov[35,53], E. Laudi[35], L. Lautner[35,108], R. Lavicka[117,38], T. Lazareva[116], R. Lea[143,24,59], J. Lehrbach[40], R.C. Lemmon[97], I. León Monzón[123], E.D. Lesser[19], M. Lettrich[35,108], P. Lévai[148], X. Li[11], X.L. Li[7], J. Lien[133], R. Lietava[114], B. Lim[17], S.H. Lim[17], V. Lindenstruth[40], A. Lindner[49], C. Lippmann[111], A. Liu[19], D.H. Liu[7], J. Liu[131], I.M. Lofnes[21], V. Loginov[96], C. Loizides[99], P. Loncar[36], J.A. Lopez[107], X. Lopez[138], E. López Torres[8], J.R. Luhder[147], M. Lunardon[28], G. Luparello[62], Y.G. Ma[41], A. Maevskaya[65], M. Mager[35], T. Mahmoud[44], A. Maire[140], M. Malaev[101], N.M. Malik[104], Q.W. Malik[20], S.K. Malik[104], L. Malinina[IV,77], D. Mal'Kevich[95], N. Mallick[51], P. Malzacher[111], G. Mandaglio[33,57], V. Manko[91], F. Manso[138], V. Manzari[54], Y. Mao[7], J. Mareš[68], G.V. Margagliotti[24], A. Margotti[55],

JHEP01(2022)106

A. Marín[111], C. Markert[122], M. Marquard[70], N.A. Martin[107], P. Martinengo[35], J.L. Martinez[128], M.I. Martínez[46], G. Martínez García[118], S. Masciocchi[111], M. Masera[25], A. Masoni[56], L. Massacrier[80], A. Mastroserio[142,54], A.M. Mathis[108], O. Matonoha[83], P.F.T. Matuoka[124], A. Matyja[121], C. Mayer[121], A.L. Mazuecos[35], F. Mazzaschi[25], M. Mazzilli[35], M.A. Mazzoni[I,60], J.E. Mdhluli[135], A.F. Mechler[70], F. Meddi[22], Y. Melikyan[65], A. Menchaca-Rocha[73], E. Meninno[117,30], A.S. Menon[128], M. Meres[13], S. Mhlanga[127,74], Y. Miake[137], L. Micheletti[61], L.C. Migliorin[139], D.L. Mihaylov[108], K. Mikhaylov[77,95], A.N. Mishra[148], D. Miśkowiec[111], A. Modak[4], A.P. Mohanty[64], B. Mohanty[89], M. Mohisin Khan[V,16], M.A. Molander[45], Z. Moravcova[92], C. Mordasini[108], D.A. Moreira De Godoy[147], I. Morozov[65], A. Morsch[35], T. Mrnjavac[35], V. Muccifora[53], E. Mudnic[36], B.J. Mughal[109], D. Mühlheim[147], S. Muhuri[144], J.D. Mulligan[82], A. Mulliri[23], M.G. Munhoz[124], R.H. Munzer[70], H. Murakami[136], S. Murray[127], L. Musa[35], J. Musinsky[66], J.W. Myrcha[145], B. Naik[135,50], R. Nair[88], B.K. Nandi[50], R. Nania[55], E. Nappi[54], A.F. Nassirpour[83], A. Nath[107], C. Nattrass[134], A. Neagu[20], L. Nellen[71], S.V. Nesbo[37], G. Neskovic[40], D. Nesterov[116], B.S. Nielsen[92], S. Nikolaev[91], S. Nikulin[91], V. Nikulin[101], F. Noferini[55], S. Noh[12], P. Nomokonov[77], J. Norman[131], N. Novitzky[137], P. Nowakowski[145], A. Nyanin[91], J. Nystrand[21], M. Ogino[85], A. Ohlson[83], V.A. Okorokov[96], J. Oleniacz[145], A.C. Oliveira Da Silva[134], M.H. Oliver[149], A. Onnerstad[129], C. Oppedisano[61], A. Ortiz Velasquez[71], T. Osako[47], A. Oskarsson[83], J. Otwinowski[121], M. Oya[47], K. Oyama[85], Y. Pachmayer[107], S. Padhan[50], D. Pagano[143,59], G. Paić[71], A. Palasciano[54], J. Pan[146], S. Panebianco[141], P. Pareek[144], J. Park[63], J.E. Parkkila[129], S.P. Pathak[128], R.N. Patra[104,35], B. Paul[23], H. Pei[7], T. Peitzmann[64], X. Peng[7], L.G. Pereira[72], H. Pereira Da Costa[141], D. Peresunko[91,84], G.M. Perez[8], S. Perrin[141], Y. Pestov[5], V. Petráček[38], M. Petrovici[49], R.P. Pezzi[118,72], S. Piano[62], M. Pikna[13], P. Pillot[118], O. Pinazza[55,35], L. Pinsky[128], C. Pinto[27], S. Pisano[53], M. Płoskoń[82], M. Planinic[102], F. Pliquett[70], M.G. Poghosyan[99], B. Polichtchouk[94], S. Politano[31], N. Poljak[102], A. Pop[49], S. Porteboeuf-Houssais[138], J. Porter[82], V. Pozdniakov[77], S.K. Prasad[4], R. Preghenella[55], F. Prino[61], C.A. Pruneau[146], I. Pshenichnov[65], M. Puccio[35], S. Qiu[93], L. Quaglia[25], R.E. Quishpe[128], S. Ragoni[114], A. Rakotozafindrabe[141], L. Ramello[32], F. Rami[140], S.A.R. Ramirez[46], A.G.T. Ramos[34], T.A. Rancien[81], R. Raniwala[105], S. Raniwala[105], S.S. Räsänen[45], R. Rath[51], I. Ravasenga[93], K.F. Read[99,134], A.R. Redelbach[40], K. Redlich[VI,88], A. Rehman[21], P. Reichelt[70], F. Reidt[35], H.A. Reme-ness[37], R. Renfordt[70], Z. Rescakova[39], K. Reygers[107], A. Riabov[101], V. Riabov[101], T. Richert[83], M. Richter[20], W. Riegler[35], F. Riggi[27], C. Ristea[69], M. Rodríguez Cahuantzi[46], K. Røed[20], R. Rogalev[94], E. Rogochaya[77], T.S. Rogoschinski[70], D. Rohr[35], D. Röhrich[21], P.F. Rojas[46], P.S. Rokita[145], F. Ronchetti[53], A. Rosano[33,57], E.D. Rosas[71], A. Rossi[58], A. Rotondi[29,59], A. Roy[51], P. Roy[113], S. Roy[50], N. Rubini[26], O.V. Rueda[83], D. Ruggiano[145], R. Rui[24], B. Rumyantsev[77], P.G. Russek[2], R. Russo[93], A. Rustamov[90], E. Ryabinkin[91], Y. Ryabov[101], A. Rybicki[121], H. Rytkonen[129], W. Rzesa[145], O.A.M. Saarimaki[45], R. Sadek[118], S. Sadovsky[94], J. Saetre[21], K. Šafařík[38], S.K. Saha[144], S. Saha[89], B. Sahoo[50], P. Sahoo[50], R. Sahoo[51], S. Sahoo[67], D. Sahu[51], P.K. Sahu[67], J. Saini[144], S. Sakai[137], M.P. Salvan[111], S. Sambyal[104], V. Samsonov[I,101,96], D. Sarkar[146], N. Sarkar[144], P. Sarma[43], V.M. Sarti[108], M.H.P. Sas[149], J. Schambach[99], H.S. Scheid[70], C. Schiaua[49], R. Schicker[107], A. Schmah[107], C. Schmidt[111], H.R. Schmidt[106], M.O. Schmidt[35,107], M. Schmidt[106], N.V. Schmidt[99,70], A.R. Schmier[134], R. Schotter[140], J. Schukraft[35], K. Schwarz[111], K. Schweda[111], G. Scioli[26], E. Scomparin[61], J.E. Seger[15], Y. Sekiguchi[136], D. Sekihata[136], I. Selyuzhenkov[111,96], S. Senyukov[140], J.J. Seo[63], D. Serebryakov[65], L. Šerkšnytė[108], A. Sevcenco[69], T.J. Shaba[74], A. Shabanov[65], A. Shabetai[118], R. Shahoyan[35], W. Shaikh[113], A. Shangaraev[94], A. Sharma[103], H. Sharma[121], M. Sharma[104], N. Sharma[103], S. Sharma[104], U. Sharma[104], O. Sheibani[128], K. Shigaki[47], M. Shimomura[86], S. Shirinkin[95], Q. Shou[41], Y. Sibiriak[91], S. Siddhanta[56], T. Siemiarczuk[88], T.F. Silva[124], D. Silvermyr[83],

JHEP01(2022)106

T. Simantathammakul[119], G. Simonetti[35], B. Singh[108], R. Singh[89], R. Singh[104], R. Singh[51], V.K. Singh[144], V. Singhal[144], T. Sinha[113], B. Sitar[13], M. Sitta[32], T.B. Skaali[20], G. Skorodumovs[107], M. Slupecki[45], N. Smirnov[149], R.J.M. Snellings[64], C. Soncco[115], J. Song[128], A. Songmoolnak[119], F. Soramel[28], S. Sorensen[134], I. Sputowska[121], J. Stachel[107], I. Stan[69], P.J. Steffanic[134], S.F. Stiefelmaier[107], D. Stocco[118], I. Storehaug[20], M.M. Storetvedt[37], P. Stratmann[147], C.P. Stylianidis[93], A.A.P. Suaide[124], T. Sugitate[47], C. Suire[80], M. Sukhanov[65], M. Suljic[35], R. Sultanov[95], V. Sumberia[104], S. Sumowidagdo[52], S. Swain[67], A. Szabo[13], I. Szarka[13], U. Tabassam[14], S.F. Taghavi[108], G. Taillepied[138], J. Takahashi[125], G.J. Tambave[21], S. Tang[138,7], Z. Tang[132], J.D. Tapia Takaki[VII,130], M. Tarhini[118], M.G. Tarzila[49], A. Tauro[35], G. Tejeda Muñoz[46], A. Telesca[35], L. Terlizzi[25], C. Terrevoli[128], G. Tersimonov[3], S. Thakur[144], D. Thomas[122], R. Tieulent[139], A. Tikhonov[65], A.R. Timmins[128], M. Tkacik[120], A. Toia[70], N. Topilskaya[65], M. Toppi[53], F. Torales-Acosta[19], T. Tork[80], S.R. Torres[38], A. Trifiró[33,57], S. Tripathy[55,71], T. Tripathy[50], S. Trogolo[35,28], V. Trubnikov[3], W.H. Trzaska[129], T.P. Trzcinski[145], B.A. Trzeciak[38], A. Tumkin[112], R. Turrisi[58], T.S. Tveter[20], K. Ullaland[21], A. Uras[139], M. Urioni[59,143], G.L. Usai[23], M. Vala[39], N. Valle[29,59], S. Vallero[61], N. van der Kolk[64], L.V.R. van Doremalen[64], M. van Leeuwen[93], P. Vande Vyvre[35], D. Varga[148], Z. Varga[148], M. Varga-Kofarago[148], M. Vasileiou[87], A. Vasiliev[91], O. Vázquez Doce[53,108], V. Vechernin[116], E. Vercellin[25], S. Vergara Limón[46], L. Vermunt[64], R. Vértesi[148], M. Verweij[64], L. Vickovic[36], Z. Vilakazi[135], O. Villalobos Baillie[114], G. Vino[54], A. Vinogradov[91], T. Virgili[30], V. Vislavicius[92], A. Vodopyanov[77], B. Volkel[35,107], M.A. Völkl[107], K. Voloshin[95], S.A. Voloshin[146], G. Volpe[34], B. von Haller[35], I. Vorobyev[108], D. Voscek[120], N. Vozniuk[65], J. Vrláková[39], B. Wagner[21], C. Wang[41], D. Wang[41], M. Weber[117], R.J.G.V. Weelden[93], A. Wegrzynek[35], S.C. Wenzel[35], J.P. Wessels[147], J. Wiechula[70], J. Wikne[20], G. Wilk[88], J. Wilkinson[111], G.A. Willems[147], B. Windelband[107], M. Winn[141], W.E. Witt[134], J.R. Wright[122], W. Wu[41], Y. Wu[132], R. Xu[7], A.K. Yadav[144], S. Yalcin[79], Y. Yamaguchi[47], K. Yamakawa[47], S. Yang[21], S. Yano[47], Z. Yasin[109], Z. Yin[7], H. Yokoyama[64], I.-K. Yoo[17], J.H. Yoon[63], S. Yuan[21], A. Yuncu[107], V. Zaccolo[24], C. Zampolli[35], H.J.C. Zanoli[64], N. Zardoshti[35], A. Zarochentsev[116], P. Závada[68], N. Zaviyalov[112], M. Zhalov[101], B. Zhang[7], S. Zhang[41], X. Zhang[7], Y. Zhang[132], V. Zherebchevskii[116], Y. Zhi[11], N. Zhigareva[95], D. Zhou[7], Y. Zhou[92], J. Zhu[7,111], Y. Zhu[7], A. Zichichi[26], G. Zinovjev[3], N. Zurlo[143,59]

Affiliation notes

[I] Deceased
[II] Also at: Italian National Agency for New Technologies, Energy and Sustainable Economic Development (ENEA), Bologna, Italy
[III] Also at: Dipartimento DET del Politecnico di Torino, Turin, Italy
[IV] Also at: M.V. Lomonosov Moscow State University, D.V. Skobeltsyn Institute of Nuclear, Physics, Moscow, Russia
[V] Also at: Department of Applied Physics, Aligarh Muslim University, Aligarh, India
[VI] Also at: Institute of Theoretical Physics, University of Wroclaw, Poland
[VII] Also at: University of Kansas, Lawrence, Kansas, United States

Collaboration Institutes

[1] A.I. Alikhanyan National Science Laboratory (Yerevan Physics Institute) Foundation, Yerevan, Armenia
[2] AGH University of Science and Technology, Cracow, Poland

JHEP01(2022)106

[3] Bogolyubov Institute for Theoretical Physics, National Academy of Sciences of Ukraine, Kiev, Ukraine
[4] Bose Institute, Department of Physics and Centre for Astroparticle Physics and Space Science (CAPSS), Kolkata, India
[5] Budker Institute for Nuclear Physics, Novosibirsk, Russia
[6] California Polytechnic State University, San Luis Obispo, California, United States
[7] Central China Normal University, Wuhan, China
[8] Centro de Aplicaciones Tecnológicas y Desarrollo Nuclear (CEADEN), Havana, Cuba
[9] Centro de Investigación y de Estudios Avanzados (CINVESTAV), Mexico City and Mérida, Mexico
[10] Chicago State University, Chicago, Illinois, United States
[11] China Institute of Atomic Energy, Beijing, China
[12] Chungbuk National University, Cheongju, Republic of Korea
[13] Comenius University Bratislava, Faculty of Mathematics, Physics and Informatics, Bratislava, Slovakia
[14] COMSATS University Islamabad, Islamabad, Pakistan
[15] Creighton University, Omaha, Nebraska, United States
[16] Department of Physics, Aligarh Muslim University, Aligarh, India
[17] Department of Physics, Pusan National University, Pusan, Republic of Korea
[18] Department of Physics, Sejong University, Seoul, Republic of Korea
[19] Department of Physics, University of California, Berkeley, California, United States
[20] Department of Physics, University of Oslo, Oslo, Norway
[21] Department of Physics and Technology, University of Bergen, Bergen, Norway
[22] Dipartimento di Fisica dell'Università 'La Sapienza' and Sezione INFN, Rome, Italy
[23] Dipartimento di Fisica dell'Università and Sezione INFN, Cagliari, Italy
[24] Dipartimento di Fisica dell'Università and Sezione INFN, Trieste, Italy
[25] Dipartimento di Fisica dell'Università and Sezione INFN, Turin, Italy
[26] Dipartimento di Fisica e Astronomia dell'Università and Sezione INFN, Bologna, Italy
[27] Dipartimento di Fisica e Astronomia dell'Università and Sezione INFN, Catania, Italy
[28] Dipartimento di Fisica e Astronomia dell'Università and Sezione INFN, Padova, Italy
[29] Dipartimento di Fisica e Nucleare e Teorica, Università di Pavia, Pavia, Italy
[30] Dipartimento di Fisica 'E.R. Caianiello' dell'Università and Gruppo Collegato INFN, Salerno, Italy
[31] Dipartimento DISAT del Politecnico and Sezione INFN, Turin, Italy
[32] Dipartimento di Scienze e Innovazione Tecnologica dell'Università del Piemonte Orientale and INFN Sezione di Torino, Alessandria, Italy
[33] Dipartimento di Scienze MIFT, Università di Messina, Messina, Italy
[34] Dipartimento Interateneo di Fisica 'M. Merlin' and Sezione INFN, Bari, Italy
[35] European Organization for Nuclear Research (CERN), Geneva, Switzerland
[36] Faculty of Electrical Engineering, Mechanical Engineering and Naval Architecture, University of Split, Split, Croatia
[37] Faculty of Engineering and Science, Western Norway University of Applied Sciences, Bergen, Norway
[38] Faculty of Nuclear Sciences and Physical Engineering, Czech Technical University in Prague, Prague, Czech Republic
[39] Faculty of Science, P.J. Šafárik University, Košice, Slovakia
[40] Frankfurt Institute for Advanced Studies, Johann Wolfgang Goethe-Universität Frankfurt, Frankfurt, Germany

JHEP01(2022)106

[41] Fudan University, Shanghai, China
[42] Gangneung-Wonju National University, Gangneung, Republic of Korea
[43] Gauhati University, Department of Physics, Guwahati, India
[44] Helmholtz-Institut für Strahlen- und Kernphysik, Rheinische Friedrich-Wilhelms-Universität Bonn, Bonn, Germany
[45] Helsinki Institute of Physics (HIP), Helsinki, Finland
[46] High Energy Physics Group, Universidad Autónoma de Puebla, Puebla, Mexico
[47] Hiroshima University, Hiroshima, Japan
[48] Hochschule Worms, Zentrum für Technologietransfer und Telekommunikation (ZTT), Worms, Germany
[49] Horia Hulubei National Institute of Physics and Nuclear Engineering, Bucharest, Romania
[50] Indian Institute of Technology Bombay (IIT), Mumbai, India
[51] Indian Institute of Technology Indore, Indore, India
[52] Indonesian Institute of Sciences, Jakarta, Indonesia
[53] INFN, Laboratori Nazionali di Frascati, Frascati, Italy
[54] INFN, Sezione di Bari, Bari, Italy
[55] INFN, Sezione di Bologna, Bologna, Italy
[56] INFN, Sezione di Cagliari, Cagliari, Italy
[57] INFN, Sezione di Catania, Catania, Italy
[58] INFN, Sezione di Padova, Padova, Italy
[59] INFN, Sezione di Pavia, Pavia, Italy
[60] INFN, Sezione di Roma, Rome, Italy
[61] INFN, Sezione di Torino, Turin, Italy
[62] INFN, Sezione di Trieste, Trieste, Italy
[63] Inha University, Incheon, Republic of Korea
[64] Institute for Gravitational and Subatomic Physics (GRASP), Utrecht University/Nikhef, Utrecht, Netherlands
[65] Institute for Nuclear Research, Academy of Sciences, Moscow, Russia
[66] Institute of Experimental Physics, Slovak Academy of Sciences, Košice, Slovakia
[67] Institute of Physics, Homi Bhabha National Institute, Bhubaneswar, India
[68] Institute of Physics of the Czech Academy of Sciences, Prague, Czech Republic
[69] Institute of Space Science (ISS), Bucharest, Romania
[70] Institut für Kernphysik, Johann Wolfgang Goethe-Universität Frankfurt, Frankfurt, Germany
[71] Instituto de Ciencias Nucleares, Universidad Nacional Autónoma de México, Mexico City, Mexico
[72] Instituto de Física, Universidade Federal do Rio Grande do Sul (UFRGS), Porto Alegre, Brazil
[73] Instituto de Física, Universidad Nacional Autónoma de México, Mexico City, Mexico
[74] iThemba LABS, National Research Foundation, Somerset West, South Africa
[75] Jeonbuk National University, Jeonju, Republic of Korea
[76] Johann-Wolfgang-Goethe Universität Frankfurt Institut für Informatik, Fachbereich Informatik und Mathematik, Frankfurt, Germany
[77] Joint Institute for Nuclear Research (JINR), Dubna, Russia
[78] Korea Institute of Science and Technology Information, Daejeon, Republic of Korea
[79] KTO Karatay University, Konya, Turkey
[80] Laboratoire de Physique des 2 Infinis, Irène Joliot-Curie, Orsay, France
[81] Laboratoire de Physique Subatomique et de Cosmologie, Université Grenoble-Alpes, CNRS-IN2P3, Grenoble, France
[82] Lawrence Berkeley National Laboratory, Berkeley, California, United States

JHEP01(2022)106

[83] Lund University Department of Physics, Division of Particle Physics, Lund, Sweden
[84] Moscow Institute for Physics and Technology, Moscow, Russia
[85] Nagasaki Institute of Applied Science, Nagasaki, Japan
[86] Nara Women's University (NWU), Nara, Japan
[87] National and Kapodistrian University of Athens, School of Science, Department of Physics , Athens, Greece
[88] National Centre for Nuclear Research, Warsaw, Poland
[89] National Institute of Science Education and Research, Homi Bhabha National Institute, Jatni, India
[90] National Nuclear Research Center, Baku, Azerbaijan
[91] National Research Centre Kurchatov Institute, Moscow, Russia
[92] Niels Bohr Institute, University of Copenhagen, Copenhagen, Denmark
[93] Nikhef, National institute for subatomic physics, Amsterdam, Netherlands
[94] NRC Kurchatov Institute IHEP, Protvino, Russia
[95] NRC "Kurchatov" Institute — ITEP, Moscow, Russia
[96] NRNU Moscow Engineering Physics Institute, Moscow, Russia
[97] Nuclear Physics Group, STFC Daresbury Laboratory, Daresbury, United Kingdom
[98] Nuclear Physics Institute of the Czech Academy of Sciences, Řež u Prahy, Czech Republic
[99] Oak Ridge National Laboratory, Oak Ridge, Tennessee, United States
[100] Ohio State University, Columbus, Ohio, United States
[101] Petersburg Nuclear Physics Institute, Gatchina, Russia
[102] Physics department, Faculty of science, University of Zagreb, Zagreb, Croatia
[103] Physics Department, Panjab University, Chandigarh, India
[104] Physics Department, University of Jammu, Jammu, India
[105] Physics Department, University of Rajasthan, Jaipur, India
[106] Physikalisches Institut, Eberhard-Karls-Universität Tübingen, Tübingen, Germany
[107] Physikalisches Institut, Ruprecht-Karls-Universität Heidelberg, Heidelberg, Germany
[108] Physik Department, Technische Universität München, Munich, Germany
[109] PINSTECH, Islamabad, Pakistan
[110] Politecnico di Bari and Sezione INFN, Bari, Italy
[111] Research Division and ExtreMe Matter Institute EMMI, GSI Helmholtzzentrum für Schwerionenforschung GmbH, Darmstadt, Germany
[112] Russian Federal Nuclear Center (VNIIEF), Sarov, Russia
[113] Saha Institute of Nuclear Physics, Homi Bhabha National Institute, Kolkata, India
[114] School of Physics and Astronomy, University of Birmingham, Birmingham, United Kingdom
[115] Sección Física, Departamento de Ciencias, Pontificia Universidad Católica del Perú, Lima, Peru
[116] St. Petersburg State University, St. Petersburg, Russia
[117] Stefan Meyer Institut für Subatomare Physik (SMI), Vienna, Austria
[118] SUBATECH, IMT Atlantique, Université de Nantes, CNRS-IN2P3, Nantes, France
[119] Suranaree University of Technology, Nakhon Ratchasima, Thailand
[120] Technical University of Košice, Košice, Slovakia
[121] The Henryk Niewodniczanski Institute of Nuclear Physics, Polish Academy of Sciences, Cracow, Poland
[122] The University of Texas at Austin, Austin, Texas, United States
[123] Universidad Autónoma de Sinaloa, Culiacán, Mexico
[124] Universidade de São Paulo (USP), São Paulo, Brazil
[125] Universidade Estadual de Campinas (UNICAMP), Campinas, Brazil

JHEP01(2022)106

[126] Universidade Federal do ABC, Santo Andre, Brazil
[127] University of Cape Town, Cape Town, South Africa
[128] University of Houston, Houston, Texas, United States
[129] University of Jyväskylä, Jyväskylä, Finland
[130] University of Kansas, Lawrence, Kansas, United States
[131] University of Liverpool, Liverpool, United Kingdom
[132] University of Science and Technology of China, Hefei, China
[133] University of South-Eastern Norway, Tonsberg, Norway
[134] University of Tennessee, Knoxville, Tennessee, United States
[135] University of the Witwatersrand, Johannesburg, South Africa
[136] University of Tokyo, Tokyo, Japan
[137] University of Tsukuba, Tsukuba, Japan
[138] Université Clermont Auvergne, CNRS/IN2P3, LPC, Clermont-Ferrand, France
[139] Université de Lyon, CNRS/IN2P3, Institut de Physique des 2 Infinis de Lyon, Lyon, France
[140] Université de Strasbourg, CNRS, IPHC UMR 7178, F-67000 Strasbourg, France, Strasbourg, France
[141] Université Paris-Saclay Centre d'Etudes de Saclay (CEA), IRFU, Départment de Physique Nucléaire (DPhN), Saclay, France
[142] Università degli Studi di Foggia, Foggia, Italy
[143] Università di Brescia, Brescia, Italy
[144] Variable Energy Cyclotron Centre, Homi Bhabha National Institute, Kolkata, India
[145] Warsaw University of Technology, Warsaw, Poland
[146] Wayne State University, Detroit, Michigan, United States
[147] Westfälische Wilhelms-Universität Münster, Institut für Kernphysik, Münster, Germany
[148] Wigner Research Centre for Physics, Budapest, Hungary
[149] Yale University, New Haven, Connecticut, United States
[150] Yonsei University, Seoul, Republic of Korea

JHEP01(2022)106